Natural Variability Dominates Precipitation Variability over the Past 800 Years in Eastern Europe

CĂTĂLIN-CONSTANTIN ROIBU,[a] VIORICA NAGAVCIUC,[b,a] CIPRIAN PALAGHIANU,[a] ANDREI MURSA,[a] COSMIN-MIHAI ANDRIESCU,[a] MIHAI-GABRIEL COTOS,[a] MARIAN-IONUȚ ȘTIRBU,[a] TOMASZ WAZNY,[c] VICTOR SFECLĂ,[a,d] AND MONICA IONITA[b,a]

[a] *Forest Biometrics Laboratory–Faculty of Forestry, Stefan cel Mare University of Suceava, Suceava, Romania*
[b] *Alfred Wegener Institute for Polar and Marine Research, Bremerhaven, Germany*
[c] *Centre for Research and Conservation of Cultural Heritage, Faculty of Fine Arts, Nicolaus Copernicus University, Toruń, Poland*
[d] *Department of Horticulture and Forestry, Technical University of Moldova, Chișinău, Republic of Moldova*

(Manuscript received 28 October 2025, in final form 27 February 2026, accepted 27 March 2026)

ABSTRACT: Tree-ring chronologies are frequently used to gain invaluable insights into past climate variability. In this study, we developed a unique 804-yr oak ring width chronology network from eastern Europe to reconstruct annual hydroclimate variability with a particular focus on the 12 July month standardized precipitation index (SPI). The SPI reconstruction captures pronounced interannual-to-multidecadal fluctuations in moisture availability, revealing sequences of persistent droughts and pluvials. These reconstructed hydroclimatic extremes align with documented historical episodes of agricultural failure, famine, and population displacement, underscoring the SPI's potential for identifying long-term climate–society linkages. Here, we show that the hydroclimate in the eastern part of Europe has largely remained stationary from 1221 to 2019, despite exhibiting substantial variability across interannual-to-multidecadal time scales. Wet years correspond to negative geopotential height anomalies over eastern Europe, promoting cyclonic flow and rainfall, while dry years align with persistent high pressure systems that suppress precipitation and shift storm tracks northward. These circulation anomalies cooccur with coherent Atlantic sea surface temperature (SST) patterns, warm subtropical and tropical anomalies during wet years, and cold anomalies during dry years, highlighting the coupled role of blocking and ocean variability in shaping multiyear droughts and floods across eastern Europe. Comparison with bias-corrected regional climate simulations suggests little change in mean annual hydroclimate through the twenty-first century, but a broadening range of possible outcomes increases risks of persistent extremes. Our study combines tree-ring reconstructions with documentary archives to place recent and future hydroclimatic extremes in a long-term context, offering critical insights for water management, agriculture, and forestry.

SIGNIFICANCE STATEMENT: The purpose of this study is to provide an eight-century reconstruction of annual hydroclimate for eastern Europe and to identify the processes and risks behind persistent extremes. Using a replication-rich oak network, we produce a robust drought record (1221–2019) that is stable across Romania, Moldova, and Ukraine. The reconstruction reveals pronounced interannual-to-multidecadal variability, including megadroughts in the fourteenth, fifteenth, and eighteenth centuries corroborated by documentary evidence that have repeatedly disrupted harvests and livelihoods. Mechanistic analyses link extremes to large-scale circulation and Atlantic sea surface temperature (SST) anomalies, with no consistent volcanic signal—implicating internal variability as the dominant driver. Projections show stable means but wider swings, heightening risks of persistent extremes and requiring adaptive water, farm, and hazard planning.

KEYWORDS: Europe; Atmosphere-ocean interaction; Teleconnections; Climate variability

1. Introduction

Climate change presents unprecedented challenges to global societies, impacting sectors ranging from agriculture and water resources to human health and infrastructure (Twardosz and Kossowska-Cezak 2013; Coumou and Rahmstorf 2012; Kreibich et al. 2022; IPCC 2021). Understanding the societal consequences of climate variability is critical for contextualizing the challenges posed by ongoing climate change and for developing effective adaptation and mitigation strategies. Historical and archaeological evidence has repeatedly demonstrated that extreme hydroclimatic events and sustained climatic shifts have contributed to the rise and fall of political systems, demographic disruptions, and the restructuring of socioeconomic practices across diverse temporal and spatial contexts (Haldon et al. 2018; Anders et al. 2013).

However, the complexity of climate–society interactions, shaped by mediating social, economic, and political conditions, necessitates high-resolution, long-term environmental records that can be meaningfully aligned with historical and archaeological archives (Jones et al. 2009; Ionita et al. 2021). Contemporary climate projections indicate that Europe, particularly its eastern and southeastern regions, will face amplified hydroclimatological

Denotes content that is immediately available upon publication as open access.

Supplemental information related to this paper is available at the Journals Online website: https://doi.org/10.1175/JCLI-D-25-0626.s1.

Corresponding authors: Viorica Nagavciuc, nagavciuc.viorica@gmail.com; Monica Ionita, monica.ionita@awi.de

DOI: 10.1175/JCLI-D-25-0626.1

variability, including more frequent droughts and heat waves (IPCC 2021; InfoClima 2024; Balting et al. 2021). These projected extremes, compounded by existing vulnerabilities and ongoing geopolitical instability, underline the importance of investigating past societal responses to climatic stressors in these regions. Reconstructions of long-term climate variability provide not only baselines for detecting anthropogenic signals but also vital analogs for understanding societal resilience and adaptation under natural climatic forcing (Nagavciuc et al. 2023b; Loon et al. 2024).

Natural paleoclimate archives, such as tree rings, offer invaluable insight into past climate conditions mostly for Common Era, extending our understanding far beyond the instrumental period (Fritts 1976). The annual resolution and wide spatial distribution of tree-ring networks allow for the reconstruction of key climate variables, including temperature, precipitation, and drought indices, providing a crucial long-term context on multicentennial time scales for recent climate change (Popa and Kern 2009; Roibu et al. 2022; Nagavciuc et al. 2022a). Although tree rings are annually resolved, their climate signal in temperate regions is typically dominated by the growing-season (spring–summer) conditions. Therefore, drought indices such as the 12-month standardized precipitation index (SPI) for July (July SPI12) are used here as an integrated measure of moisture availability up to the peak of the growing season rather than as a strictly annual target. Specifically, long-lived oak (*Quercus* spp.) species in Europe have proven to be highly sensitive to climatic variations, yielding precisely dated and annually resolved chronologies that can span multiple centuries and even millennia (Roibu et al. 2021; Nagavciuc et al. 2023a; Sochová et al. 2021; Bose et al. 2021; Wazny and Eckstein 1991).

Despite the well-established field of dendroclimatology in Europe, the availability and spatial coverage of long, well-replicated, precisely dated tree-ring chronologies suitable for high-resolution hydroclimate reconstructions remain comparatively sparse in eastern Europe compared with western Europe, and recent efforts have aimed to help bridge this regional gap (Nagavciuc et al. 2022a; Köse et al. 2013; Levanič et al. 2013; Nagavciuc et al. 2019a; Roibu et al. 2022). The region's vulnerability to climate extremes, particularly severe droughts and heat waves, which have historically impacted agricultural productivity and societal stability, highlights the need to develop long-term, tree-ring paleoclimate reconstructions (Kreibich et al. 2022; Dobrovolný et al. 2010; Ionita and Nagavciuc 2021; Ionita et al. 2025a, 2024). Moreover, extending the climate record further back in time enables the detection of past periods of extreme climate variability, assessing their frequency and magnitude and investigating their potential impact on historical societal development (Luterbacher et al. 2012).

Long tree-ring paleoclimate reconstructions are essential in eastern Europe due to their susceptibility to climatic extremes, like droughts and heat waves (Cook et al. 2015; Ionita et al. 2025a, 2024; Ionita and Nagavciuc 2024). Extending these records allows for quantifying past extreme climate variability and assessing its influence on historical societal trajectories. Understanding the intricate relationship between climate variability and societal changes is critical for building resilience to current climate challenges. Historical records often document periods of societal upheaval, migration, and economic shifts that coincided with significant climate anomalies (Brázdil et al. 2022; Zhang et al. 2011; Brázdil et al. 2010; Guillet et al. 2020; Stothers 1999). By reconstructing past climate variability at high resolution and comparing it with historical sources of societal changes in eastern Europe, we can gain valuable insights into the potential pathways through which climate can influence human systems and identify critical thresholds of vulnerability and adaptation.

Therefore, this study aims to reconstruct past drought variability (July SPI12) over the eastern part of Europe for period 1221–2019 Common Era (CE) based on annually resolved oak tree-ring chronology and to analyze the link between tree-ring width variability and large-scale atmospheric circulation. Furthermore, we explore the relationship between extreme climatic events and documented societal changes in eastern Europe during this period, shedding light on the long-term interplay between environmental and human history. Also, we aim to investigate the future drought characteristics and their associated risks in Romania through the twenty-first century by analyzing an ensemble of bias-corrected regional climate simulations under different representative concentration pathways (RCPs) (Dumitrescu et al. 2023).

2. Data and methods

a. Study area

The study area spans eastern Europe, extending from the easternmost part of the Carpathian chain to the Dniester River (Fig. 1). The study area features forests dominated by beech (*Fagus sylvatica* L.) and oak species, occurring in both pure and mixed stands (Stănescu 1979; Horeanu 1996). The pedunculate oak (*Quercus robur* L.) and sessile oak [*Quercus petraea* (Matt.) Liebl.] are the most prevalent oak species within this area (Horeanu 1996). *Q. petraea* is typically associated with higher altitudes and rocky soils, while *Q. robur* exhibits a wider distribution across plains, where it thrives in thick layers of loose, fertile soils (Ellenberg 2009). Across this broader region, both oak species face diverse environmental conditions, predominantly growing under warm and arid climatic regimes, particularly in lowland areas, along an altitudinal gradient ranging from 178 to 523 m MSL (Ellenberg 2009; Horeanu 1996). From the environmental perspective, the studied region is characterized by a temperate continental climate. This climatic regime is defined by cold winters and warm-to-hot summers, with summer moisture limitations often strongest in the extra-Carpathian/eastern lowlands. The multiannual-mean temperatures exhibit a gradient, ranging from +6° to +8°C in the northern regions and from +9° to +10°C in the southern regions. Annual precipitation exhibits a corresponding spatial variation, with values ranging from 500 to 800 mm in the north and 400–500 mm in the south. Seasonally, precipitation is typically concentrated in late spring–early summer, followed by a relative precipitation minimum in mid-to-late summer (July–August), when evaporative demand is highest and drought impacts on vegetation growth are most likely. In line with this, recent analyses for Romania document strong interannual-to-decadal variability in summer hydroclimate, alongside an increase in the frequency/duration of summer heat waves after the 1990s and a

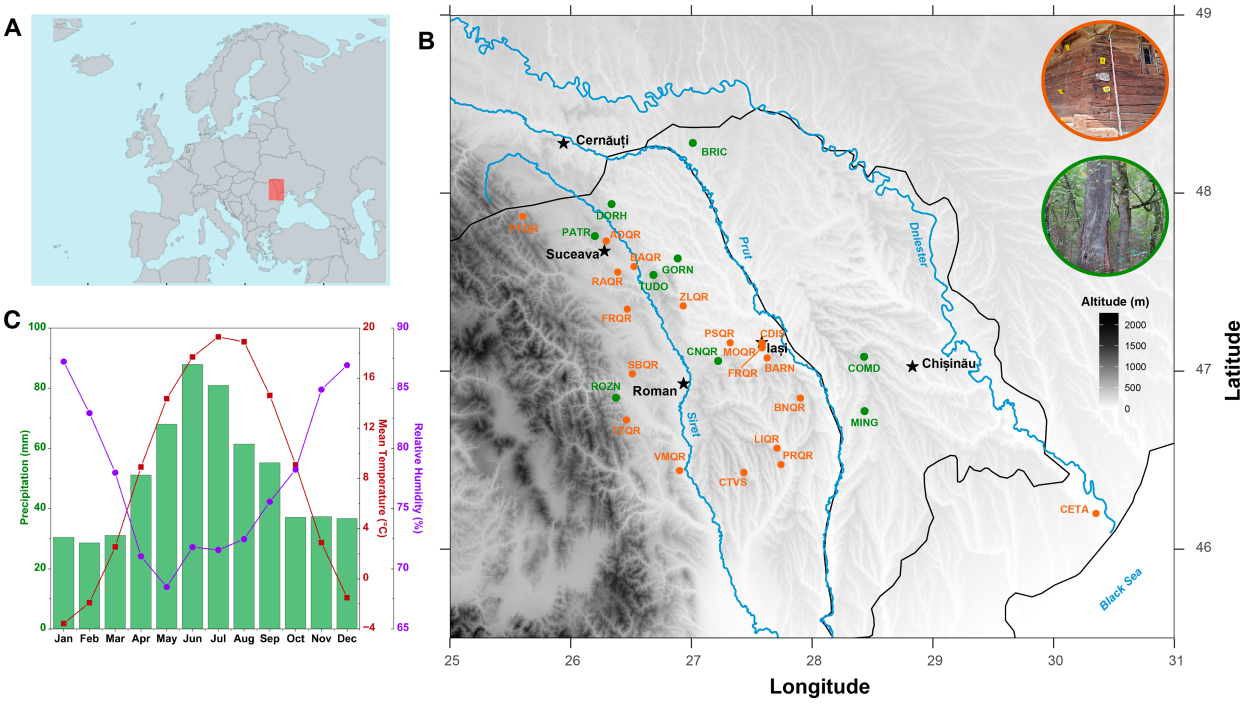

FIG. 1. Study area and sampling sites. (a) General location with a focus on the study area (red rectangle). (b) Sampling area (with green—living oak tree sampling sites—and with orange—archaeological oak wood sites). (c) Climatology of precipitation, mean temperature, and relative humidity at the Iași meteorological station.

tendency toward drier late-summer conditions (Nagavciuc et al. 2022b). At decadal scale, recent decades (post-1990) include more frequent dry-summer conditions than earlier periods, consistent with the broader shift toward hotter and drier summers highlighted for Romania (InfoClima 2024; Ionita et al. 2025a; Nagavciuc et al. 2022b). Long-term trends over the past century indicate an expansion of arid zones, highlighting a progressive shift in regional hydrological conditions (Ionita and Nagavciuc 2021).

b. *Tree-ring dataset*

To reconstruct past interannual-to-multicentennial drought variability, we used the Suceava oak chronology, which comprises 554 samples, including 183 living trees and 371 historical timbers, spanning the period 1216–2019 CE (Roibu et al. 2021). The chronology was constructed on the two dominant oak species in the region, specifically English oak (*Quercus robur*) and sessile oak (*Quercus petraea*). Between both species, there are no differences from the anatomical point of view (Ruffinatto and Crivellaro 2019; Feuillat et al. 1997), and their response to hydroclimatic conditions seems to be similar (Tegel et al. 2010; Friedrichs et al. 2009; Cufar et al. 2014). Additional details about the development of the Suceava oak chronology and its associated statistical analyses are provided in Roibu et al. (2021). To remove the biological age-related growth trend and nonclimatic signals from individual tree-ring series, we applied the regional curve standardization (RCS) method (Esper et al. 2003), one of the standard detrending techniques used in climatic reconstructions (Büntgen et al. 2011b). We used the RCS indices because of their higher capacity to preserve the full spectrum of climatic variability and reduce bias caused by individual tree growth trends (Briffa et al. 1992; Esper et al. 2016; Homfeld et al. 2024). Additionally, due to these capabilities, RCS indices are particularly useful for studying the recurrence intervals of extreme climatic events. The variance of the RCS index was stabilized using a 31-yr moving average approach (Osborn et al. 1997), which corrects for artificial variance changes driven by varying sample depth over time (Frank et al. 2007). The chronology statistics, mainly the expressed population signal (EPS) (Wigley et al. 1984) and the interseries correlation, rbar, together with sample replication, have demonstrated that the entire time interval can be used to reconstruct past hydroclimate variability and fulfil the paper's aim (Fig. 2).

c. *Climate data and TRW index relationship*

The hydroclimatic potential of the oak chronology was tested by performing Pearson correlation analyses between the tree-ring width (TRW) index and main climatic parameters (precipitation and mean temperature) using both monthly gridded data obtained from the CRU Time Series (TS) v. 4.09 dataset (Harris et al. 2020), covering the period 1901–2019, as well as station-based data (i.e., Iași meteorological station, 1895–2019). SPI was computed based on the monthly precipitation (PP) data, extracted from the CRU TS v. 4.09 dataset (Harris et al. 2020), as well as from Iași meteorological station, using the R package standardized precipitation evapotranspiration index (SPEI) (https://cran.r-project.org/web/packages/SPEI/index.html). For this study, we examined the correlation between the TRW index

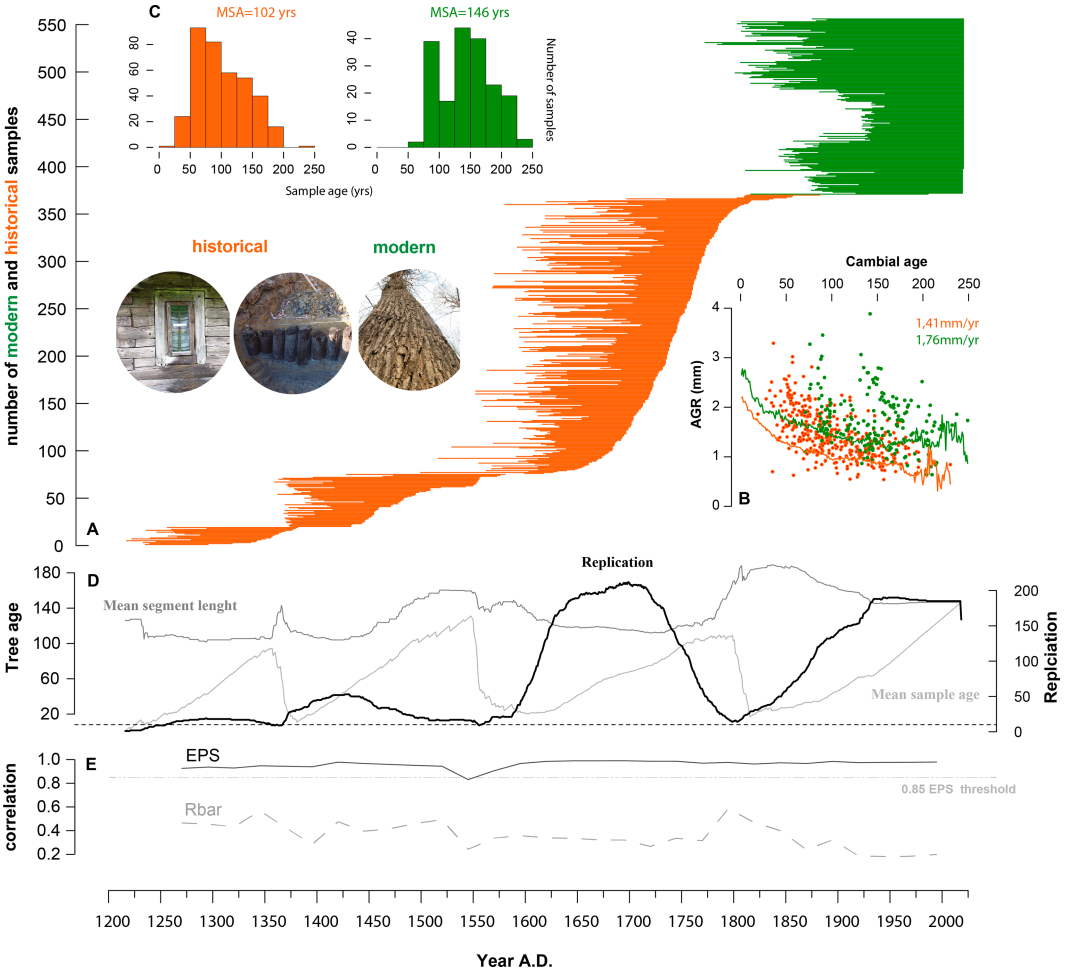

FIG. 2. Chronology characteristics. (a) Temporal distribution of 183 living oak trees (dark green) and 371 archaeological oak samples (orange), aligned to the outermost ring; (b) relationship between mean segment length and average growth rate (AGR) for modern and historical samples (dots) and mean growth variation with cambial age (lines); (c) histograms of sample length (age) for living and archaeological material, mean sample age (MSA); (d) temporal variations in mean sample length (dark gray), MSA (light gray), and replication (black); and (e) 50-yr moving statistics of interseries correlation (rbar) and EPS.

and the SPI at various time scales (1, 3, 6, 9, 12, and 24 months—SPI1, SPI3, SPI6, SPI9, SPI12, and SPI24, respectively) and for different months (January–December of the current year). This investigation allowed us to identify the most relevant period for the drought reconstruction.

The spatial correlation, at the European level, between the TRW index and SPI was examined using the stability-map approach (Ionita et al. 2008) and the linear correlation analysis. The stability methodology is successfully applied not only in seasonal forecasts of European rivers and Antarctic Sea ice (Ionita et al. 2008, 2015, 2018; Ionita 2024) but also in dendrochronological studies (Nagavciuc et al. 2019b; Roibu et al. 2022; Nagavciuc et al. 2019a). This method allows us to explore the stationarity of the long-term relationship between our proxy and gridded climate data. To identify stable predictors, we analyzed the temporal variability of the correlation between tree-ring parameters and gridded climatic data using a 31-yr moving window spanning the 1901–2019 period. A correlation was considered stable in regions where the relationship between the tree-ring parameter and the gridded data remained significant (exceeding the 90% confidence level) for more than 80% of the length of the moving window analyses. Essentially, this methodology aims to identify geographical areas where the correlation between the TRW index and SPI remains consistent throughout the study period.

Stability maps are superior to single-period correlation maps as they provide a more robust assessment of teleconnections and effectively filter out correlations that are either sample specific or regime dependent by explicitly testing the persistence of local associations between a target series and each grid point across multiple moving windows or subsamples. This process retains only the temporally consistent teleconnections that are reliable for predictive modeling. Moreover, by adding this persistence criterion and, where possible, coupling it with field-significance

control, stability maps mitigate the multiple testing problem and the inflation of nominal significance caused by spatial and temporal dependences, which routinely leads pointwise correlation maps to overstate evidence.

d. Reconstruction model

For drought reconstruction in eastern Europe, we utilized July SPI12, spanning from 1895 to 2019. The reconstruction model was developed using a linear regression model within the R package *treeclim* (Zang and Biondi 2015). To mitigate regression-based variance reduction in the reconstruction, the RCS chronology was scaled with the July SPI12 mean and standard deviation (Esper et al. 2005). To assess predictive skill, we evaluated the reconstruction over the 124-yr instrumental period (1896–2019) using split-sample calibration–verification tests. We calibrated the model in 1896–1957 and verified it in 1958–2019 and then repeated the procedure with the periods reversed to test temporal stability. The final reconstruction model was subsequently fitted using the full 1896–2019 dataset. To evaluate the model's explanatory power, predictive accuracy, and overall performance, we computed the coefficient of determination (R2), the reduction in error (RE), and the coefficient of efficiency (CE). A crucial criterion for model acceptance was RE and CE values greater than 0 (Briffa et al. 1992; Cook and Kairiukstis 1990). Additionally, the Durbin–Watson (DW) statistic was employed to check for trends in the residuals (Durbin and Watson 1950). Extreme years are defined as those when the July SPI12 index exceeds +2 (extremely wet) or falls below −2 (extremely dry), whereas wet and dry years correspond to July SPI12 values between +1.5 and +2 and between −1.5 and −2, respectively.

e. Documentary sources

Eastern Europe is a region with a limited collection of documentary evidence regarding climate, its impacts, and societal responses. Turmoiled historical conditions, including continuous migratory incursions during the first millennium and prolonged warfare following the formation of national states, largely obstructed the systematic documentation of climatic phenomena (Teodoreanu 2017). Weather phenomena were primarily documented by local chroniclers, monks, priests, foreign travelers, and diplomats. These observers offered broader descriptions of climate, and their records were mainly intended to explain variations in agricultural yields (Cernovodeanu and Binder 1993). In this context, the historical database was developed based on diverse archive sources, chronicles, and historical annals. Each extreme year identified in our reconstruction was linked with relevant historical records documenting the occurrence of natural disasters, famine, agriculture production, wildfires, disease outbreaks, and locust invasion, as well as monthly and annual variations in main climatic parameters, like precipitation and temperature (Teodoreanu 2017; Mihailescu 2004; Topor 1963; Dudaș 1999; Cernovodeanu and Binder 1993). Moreover, as an additional verification step, multiple high-resolution precipitation reconstructions over central Europe are used (Wilson et al. 2005; Dobrovolný et al. 2018b; Büntgen et al. 2011b,a; Brázdil et al. 2002). Eastern Europe (Levanič et al. 2013; Cook et al. 2024, 2020; Nagavciuc et al. 2022a; Solomina et al. 2005) and the Aegean region (Touchan et al. 2005; D'Arrigo and Cullen 2001; Griggs et al. 2007; Akkemik et al. 2005) were used to enhance the robustness of the analysis and enable a comprehensive comparative assessment of regional hydroclimatic variability.

To better understand the links between climate variability and societal changes, such as demographic shifts, regional migrations, disease outbreaks (e.g., plague), and famines, we draw on an expanding body of evidence indicating that climate forcing has been a key driver of historical crises. However, the scarcity of high-resolution paleoclimatic data prior to 800 years ago poses challenges in accurately reconstructing these climate–society interactions, thereby constraining our ability to establish direct correlations with human history (Büntgen et al. 2011a; Ljungqvist et al. 2021; Brázdil et al. 2013). To mitigate this limitation, we have linked extreme hydroclimatic events with societal changes in eastern Europe, providing a refined perspective on the interplay between climate and human societies.

On the other hand, many past climatic fluctuations were driven by factors such as volcanic activity (Fischer et al. 2007; Atwell 2001; Esper et al. 2013). To further illustrate the magnitude of these hydroclimatic anomalies and explore their underlying drivers, we incorporated major volcanic eruptions (Toohey and Sigl 2017) as potential external climate-forcing events. These high-impact eruptions provide critical chronological markers that may have contributed to abrupt climatic shifts and societal transformations (Guillet et al. 2020; Stothers 1999). By aligning the timing of these eruptions with episodes of environmental and societal stress, we highlight their potential role in amplifying hydroclimatic extremes and shaping historical patterns of human vulnerability and response across eastern Europe.

f. Large-scale atmospheric circulation

The influence of the large-scale atmospheric circulation on the variability of wet/dry periods has been investigated using the monthly means of geopotential height at 500 mb (1 mb = 1 hPa) (Z500), zonal wind at 500 mb (U500), and meridional wind at 500 mb (V500) from the Twentieth Century Reanalysis (V3) dataset (Compo et al. 2011, 2006; Slivinski et al. 2019) on a 2 × 2 grid, over the 1836–2015 CE period. For the sea surface temperature (SST), we used the Extended Reconstructed SST (ERSST) dataset V5 (spatial resolution 2 × 2), covering the 1854–2020 period (Huang et al. 2018). To identify connections between the large-scale oceanic (SST) and atmospheric circulation (Z500) and the variability of our reconstructed July SPI12 drought index, we used the composite map methodology (Storch and Zwiers 1999). To construct these maps, we selected years when the reconstructed SPI12 July time series value was either above 1 (representing wet years) or below −1 (representing dry years). This threshold offered a balance between the strength of climate anomalies and the number of maps that met our criteria. The composite analysis is a widely accepted method for understanding physical mechanisms and developing statistical prediction models (Storch and Zwiers 1999). To isolate the specific climate signal, we subtract the long-term climatological mean from the composite mean. To ensure these patterns are not the result of random internal climate variability, we apply a two-tailed Student's

t test. The significance at each grid point is determined by comparing the mean of the composite group against the mean of the remaining population. Only regions where the difference is significant at the 95% confidence level ($p < 0.05$) are shaded or contoured in the final maps. This highlights the centers of action, such as Rossby wave trains or specific SST teleconnection patterns, that physically drive the drought or pluvial conditions. We must mention that the composite map analysis has also been performed on the raw RCS time series (not shown) to test the robustness of the results. Since the results are almost identical, in this study, we only show the large-scale patterns associated with the reconstructed SPI12 July index. The composite map analysis and the stability maps have been performed in MATLAB2024b.

3. Results

a. The chronology skills and climate growth relationship

Our long oak chronology shows a high potential for dendroclimatological and climate reconstruction analyses, as supported by the robust statistical values of EPS, rbar, and associated parameters. The mean rbar value for the entire dataset is 0.35, reflecting the high temporal homogeneity of the tree-ring material (Fig. 2). This value is notably higher than that observed in other European hydroclimatic reconstructions (0.25) and comparable to Asian chronologies (0.38) (Ljungqvist et al. 2020). The observed homogeneity is likely to result from the inclusion of historical construction timber and living trees from a large region with similar environmental conditions and a strong continental influence (Ljungqvist et al. 2020). Another potential factor contributing to the high chronology homogeneity is the relatively limited timber trade in the region compared to western and central Europe (Roibu et al. 2021; Büntgen et al. 2011a; Ljungqvist et al. 2020). Historically, large oak forests once covered the area with timber primarily used for local construction needs and offered as tribute to the Ottoman Empire (Giurescu 1976). Also, sample replication plays a critical role in climate reconstruction, significantly enhancing the reliability and accuracy of the results. Its value extends beyond climatic reconstructions, offering critical insights into societal responses to environmental change. Fluctuations in sample replication can reveal periods of economic crisis, political instability, or prolonged conflicts, deepening our understanding of how societies have adapted to shifting environmental and political conditions over time (Büntgen et al. 2011a; Roibu et al. 2021; Tegel et al. 2010). Our chronology includes a total of 554 samples, which is less extensive compared with some other European reconstructions (Büntgen et al. 2011a; Tegel et al. 2010). However, the sample depth consistently exceeds 10 over 1250 CE. Overall, the mean replication exhibits a pronounced increase after cc. 1650 CE. The subsequent decline in sample depth following ~1800 CE stems from two possible causes: A shift in construction practices from oak to coniferous wood and the limited availability of very old oak trees. This reduction may, in part, be associated with the Treaty of Adrianople (1829 CE), which facilitated the freedom to trade cereals and timber between Romanian Principalities and western European countries (Geacu and Grigorescu 2022; Constantin 2015). Consequently, large areas of oak forests were deforested for rapid agricultural development, while oak timber—esteemed from that moment onward as a noble wood—acquired increased trade value, preferentially used for furniture production rather than for common construction purposes.

The strong internal coherence over the past eight centuries underscores a stable climatic influence on oak growth in eastern Europe, as demonstrated by the running EPS consistently exceeding the quality threshold of 0.85 (Wigley et al. 1984; Briffa et al. 1983). High first-order autocorrelation [AC (1)] indicates a significant carry-over effect, where previous year's environmental conditions strongly influenced current-year growth. Together with the mean interseries correlation (rbar) and signal-to-noise ratio (SNR), these metrics confirm the high sensitivity of Suceava oak chronology to environmental variability and underscore its robustness for high-resolution climatic reconstructions.

The hydroclimatic potential of the oak chronology was tested by performing Pearson correlation analyses between the TRW index and main climatic parameters (precipitation and mean temperature) using one of the longest meteorological stations located over the study site (i.e., Iași meteorological station, 1895–2019 CE; Fig. 1). Considering the sensitivity of the TRW index to precipitation and temperature, we also investigated its relationship with drought indices, namely, SPI. In the case of precipitation and mean air temperature, weak and insignificant correlations have been found (Figs. S1a,b in the online supplemental material). The highest correlation has been obtained between July SPI12 and the residual chronology (RCS, $r = 0.63$, $p < 0.001$; Fig. S3b), which indicates that long-term drought has a strong influence on the oak growth (Nagavciuc et al. 2023a). We have to mention that we tested different accumulation periods for the SPI index (i.e., from 1 to 12 months), but only the correlations for SPI3, SPI6, SPI9, and SPI12 are shown in the current study (Fig. S2 and S3). The significant relationship with long-term drought indicators (e.g., SPI12) indicates that despite their affinity for mesic conditions, oaks exhibit high drought tolerance through deep root systems, mycorrhizal associations, and efficient groundwater uptake. Here, July SPI12 denotes the standardized precipitation index accumulated over the 12 months ending in July (i.e., from August of the previous year to July of the current year). Thus, it represents a 12-month integrated precipitation anomaly with a clear summer endpoint, rather than a purely "summer-only" or strictly "annual" signal. Considering these findings, our result has a strong physiological background and highlights the critical role of these adaptations in oak sensitivity to prolonged droughts (Mikac et al. 2018; Abrams 1990; Skiadaresis et al. 2021; Allen 2015; Petritan et al. 2021). Ecologically, the strongest growth response is expected when this long-term moisture deficit culminates around June–July, coinciding with peak cambial activity and maximum evaporative demand, when cumulative deficits most strongly constrain plant-available water. Extended and excessive drought conditions lead to reduced groundwater levels, triggering a series of physiological, anatomical, and ecological responses, including low growth rates reflected in narrower tree-ring width (Früchtenicht et al. 2021; Mikac et al. 2018; Roibu et al. 2020; Tumajer and Treml 2016; Fonti and García-González 2008; Drobyshev et al. 2008; Lv et al. 2022).

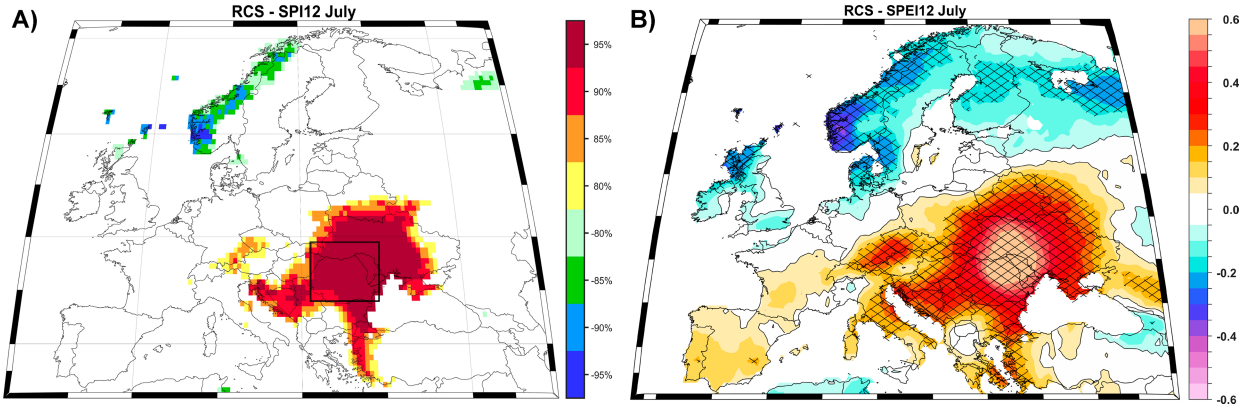

FIG. 3. (a) Stability map RCS vs SPI12 July and (b) correlation map RCS vs SPI12 July. In (a), regions where the correlation is stable, positive, and significant, for at least 80% windows, are shaded in dark red (95%), red (90%), orange (85%), and yellow (80%). The corresponding regions where the correlation is stable, but negative, are shaded in dark blue (95%), blue (90%), green (85%), and light green (80%). In (b), hatching highlights significant values at a 95% confidence level. Analyzed period: 1901–2019.

b. Spatial stability of the drought signal

Next to the local correlations (i.e., RCS vs station-based climatic parameters), we also evaluated the spatiotemporal stability of hydroclimatic signals using stability maps and linear correlation between the RCS chronology and the gridded SPI drought index at the European level. This analysis examined whether the RCS chronology exhibits significant relationships not only locally but also across a broader spatial domain. This analysis covered the period 1901–2019 CE and was performed using the CRU TS v. 4.09 data (Harris et al. 2020). To identify the optimal spatiotemporal interval, we performed the stability map analysis from September of the previous year to October of the current year (Fig. S4). The results from the stability maps show a positive, stable, and significant correlation between our RCS chronology and the SPI drought index across Romania, the Republic of Moldova, and the central and western parts of Ukraine (Fig. S4). This significant and stable correlation is particularly evident for a 12-month cumulative period, spanning from August of the previous year to July of the current year (Fig. 3a, Figs. S3 and S4). This finding aligns with previous research, confirming that a 12-month accumulation period provides the most robust signal for reconstructing drought variability in eastern Europe and that oak tree growth is significantly impacted by prolonged drought events (Nagavciuc et al. 2023a). We also tested the relationship between the TRW and SPI by employing a simple linear correlation map between the RCS chronology and the July SPI12 drought (Fig. 3b). The correlation map has a similar structure to the stability map, but the regions with significant correlations are more extended compared to the ones identified in the stability map. We observed a significant and positive correlation over a large region including Romania, the Republic of Moldova, Ukraine, Belarus, eastern Poland, Slovakia, Hungary, Serbia, and Bulgaria. On the other hand, a significant and negative correlation was found over Norway (Fig. 3b). These findings highlight the value of the stability map approach in identifying areas with strong and temporally stable correlations, which are crucial for reliable paleoclimate reconstructions.

c. Hydroclimatic reconstruction

As previously mentioned, to reconstruct hydroclimatic variability in eastern Europe over the past 804 years, we used the July SPI12 calculated from observations at the Iași meteorological station (Fig. 1), which provides a continuous record from 1894 to 2019 CE. We also used stability maps to identify the proper lag and SPI scale for our study, but for the final reconstruction, we used station data, as the uncertainties in the observational records measured at the meteorological station are significantly lower compared to the uncertainties from the gridded data. Moreover, the station-based data have a longer temporal extent compared to the CRU data, which allows us to better calibrate/validate our statistical parameters associated with our reconstruction. The correlation coefficient between the RCS chronology and July SPI12 at Iași station is 0.63 ($p < 0.001$; Fig. S3), and the correlation coefficient between the TRW index and July SPI12 based on CRU data (black square in Fig. 3a) is 0.62 ($p < 0.001$). The running correlation analysis between the RCS chronology and July SPI12 (Fig. 4a) revealed that the climate–growth relationship stays fairly stable and significant over time, with a decline to 0.44 between 1914 and 1945 CE, while the highest correlation ($\sim r = 0.75$) was observed during the period 1983–2013 CE, indicating a strong coherence between tree-ring indices and the target data (Fig. 4a). These findings are consistent with other dendroclimatic models developed under comparable environmental conditions (Mészáros et al. 2022; Roibu et al. 2020; Friedrichs et al. 2009; Nechita et al. 2019; Árvai et al. 2018; Sochová et al. 2024, 2021; Petritan et al. 2021). However, they differ from certain central European models, where a loss of coherence in the climate–growth relationship has been observed in recent decades (Dobrovolný et al. 2018b).

The SPI12 July at Iași station was used as the predictand, and the RCS chronology was used as the predictor (Fig. 4b). Reconstruction skills were evaluated in the forward and reverse models. Overall, the reconstruction skills indicate a well-calibrated model with minimal bias and no evidence of overfitting to the calibration data, being comparable with other hydroclimatic

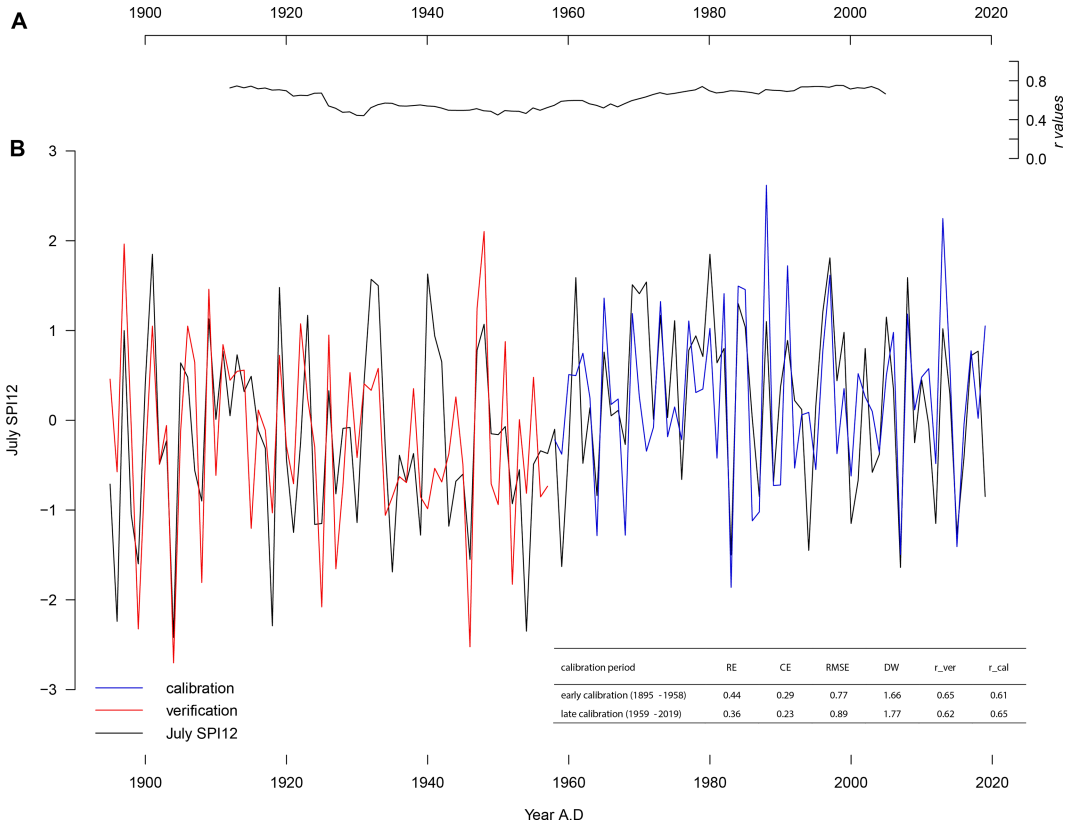

FIG. 4. Model skill: (a) Running correlation (31-yr window) between the scaled RCS chronology and the July SPI12 time series for the 1895–2019 period; (b) calibration–verification model for July SPI12, black line—measured data—and red and blue lines—reconstructed July SPI_12 for calibration and verification periods, respectively; model skill metrics are summarized in the accompanying table: RMSE = root-mean-square error, r_ver = verification-period correlation coefficient, and r_cal = calibration-period correlation coefficient.

reconstructions (Cook and Kairiukstis 1990; Fritts 1976). Thus, the model seems to perform better when it is calibrated on the more recent period (1959–2019 CE), likely due to more accurate climate data and the model's ability to capture recent climatic trends. Specifically, shifts in precipitation variability, an increase in the frequency of extreme events, or changes in the frequency and duration of dry or wet spells can increase the oak's sensitivity to climate variability. The difference in metrics also highlights that the early period (1895–1958 CE) might be more challenging for the model due to changes in climate dynamics over time, potentially influenced by climate change and shifts in precipitation variability, as oaks are more sensitive to prolonged droughts (Petritan et al. 2021; Nagavciuc et al. 2023a).

The calibration and verification models successfully passed all conventional verification tests in both forward and reverse modes. The positive values obtained for the RE and CE in both modes demonstrate the reconstruction's strong predictive skills (Fig. 4). Furthermore, a DW value near 2 indicates low to no autocorrelation, further supporting the model's robustness. These statistical results confirm that the linear regression model employed is reliable and possesses high predictive skill for reconstructing the July SPI12 over eastern Europe. Consequently, this developed model is suitable for reconstructing past long-term drought variability.

Our reconstruction goes back to 1221 CE and captures climatic variations at interannual and multidecadal scales. Although EPS and rbar values remain relatively high due to the moving-window calculation, the actual sample replication before 1250 CE is lower. Therefore, this early segment of the reconstruction is associated with greater uncertainty and should be interpreted with caution. For the entire reconstructed period, 15 extreme wet years, 27 extreme dry years, 33 wet years, and 38 dry years were found (Fig. 5a, Table 1). However, they are not uniformly distributed over time, with several distinct periods being identified (Figs. 5b,c).

The early period (1221–1300 CE) was predominantly wet (4 extreme wet, 5 wet, and 4 dry years), followed by a dry phase between 1300 and 1500 CE (2 extreme wet, 9 wet, 8 extreme dry, and 10 dry years). The sixteenth century showed generally both wet and dry conditions (1 extreme wet, 6 wet, 2 extreme dry, and 4 dry years), whereas the period 1600–1800 CE was strongly dry (3 extreme wet, 6 wet, 8 extreme dry, and 11 dry years). The nineteenth century was balanced (2 extreme wet, 6 wet, 2 extreme dry, and 5 dry years), and the modern era (twentieth–twenty-first centuries) was characterized by dry climate and precipitation deficit (3 extreme wet, 1 wet, seven extreme dry, and 4 dry years).

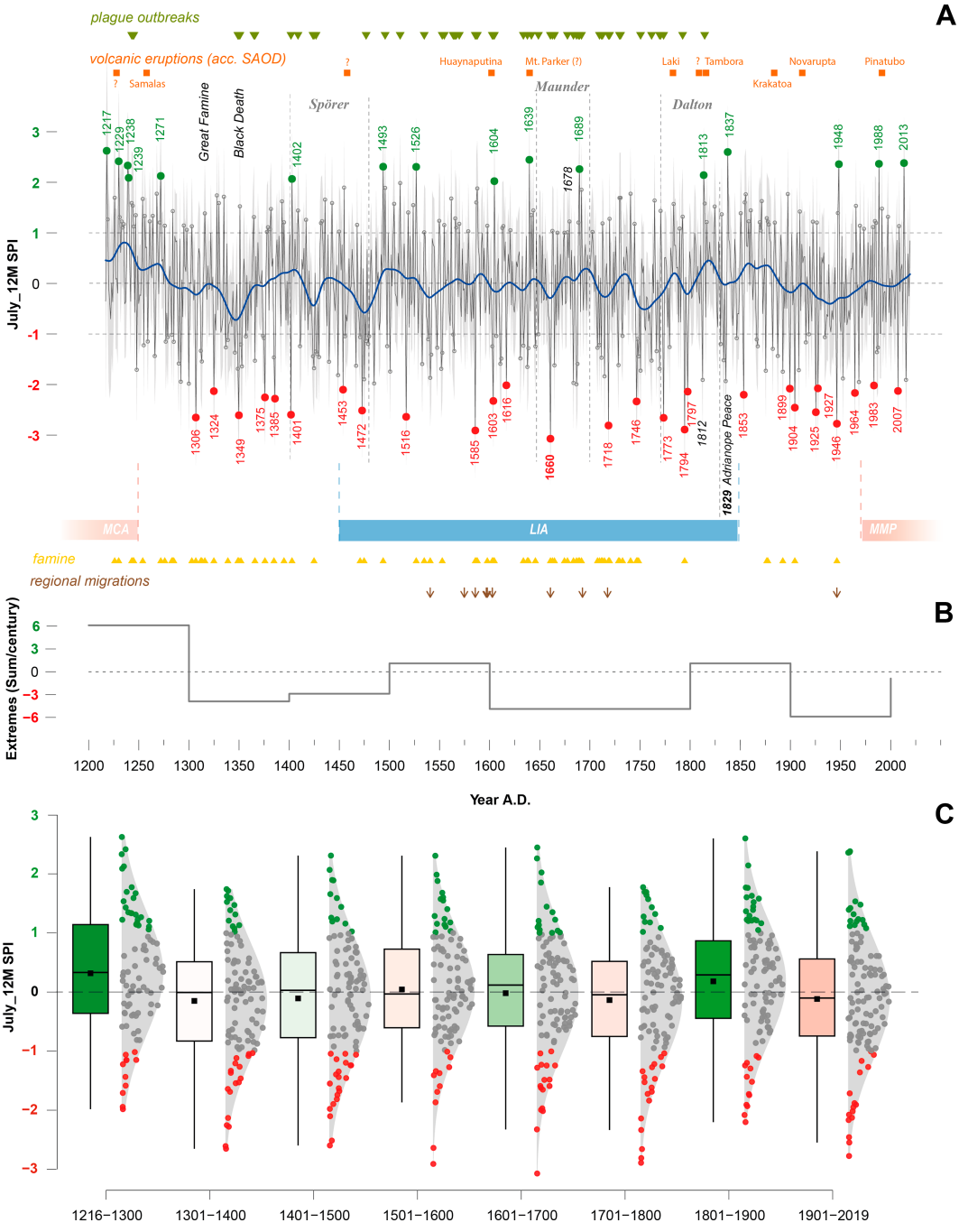

FIG. 5. Drought temporal variability: (a) Annual July SPI12 reconstruction for the period 1221–2019, overlaid with major volcanic eruptions [based on stratospheric aerosol optical depth (SAOD); Toohey and Sigl 2017], known plague outbreaks (Cernovodeanu and Binder 1993; Mihailescu 2004), and regional migrations (Mihailescu 2004; Cernovodeanu and Binder 1993). The dark-blue line represents a 31-yr low-pass filter, red dots indicate extreme dry years (SPI < -2), and green dots indicate extreme wet years (SPI > 2); (b) centennial variability of extreme hydroclimatic events; (c) boxplots and Gaussian-derived frequency distributions (gray polygons) of reconstructed July SPI12 values across centuries during 1221–2019 CE.

TABLE 1. The year's corresponding to the extreme wet: July SPI12 index exceeds +2, extremely dry: July SPI12 index falls below −2, wet: July SPI12 values between +1.5 and +2, and dry: July SPI12 values between −1.5 and −2, over the 1221–2019 CE period.

Extreme wet years Wet years	Extreme dry years Dry years
1229, 1238; 1239, 1271; 1402, 1493; 1526, 1604; 1639, 1689; 1813, 1837; 1948, 1988; 2013	1306, 1324; 1349, 1375; 1385, 1401; 1453, 1472; 1516, 1585; 1603, 1616; 1660, 1718; 1746, 1773; 1794, 1797; 1853, 1899; 1904, 1925; 1927, 1946; 1964, 1983; 2007
1225, 1242; 1243, 1253; 1267, 1327; 1329, 1334; 1350, 1392; 1435, 1442; 1454, 1495; 1504, 1510; 1523, 1561; 1586, 1587; 1691, 1729; 1730, 1740; 1764, 1783; 1814, 1824; 1854, 1855; 1871, 1897; 1965	1247, 1289; 1291, 1299; 1312, 1348; 1352, 1365; 1424, 1439; 1448, 1466; 1474, 1484; 1500, 1532; 1540, 1551; 1610, 1637; 1664, 1683; 1686, 1687; 1714, 1728; 1750, 1761; 1769, 1812; 1833, 1835; 1875, 1892; 1908, 1952; 1968, 2015

4. Discussion

a. *Hydroclimatic regimes and drivers*

This study presents the first tree-ring-based reconstruction of July SPI12 for eastern Europe, extending back to 1221 CE. It provides annually resolved hydroclimatic information for periods and regions largely lacking written documentation, thereby filling a key gap in the long-term understanding of moisture variability. Unlike previous efforts limited to seasonal indices or smaller subregions, this reconstruction captures multicentury drought and wetness variability on an annual scale. Importantly, it delivers genuinely new hydroclimatic evidence for historically undocumented intervals and accurately reproduces numerous recorded extreme events, offering a robust environmental context for past societal changes. The pronounced hydroclimatic fluctuations observed at the end of the Medieval Climate Anomaly (Xoplaki et al. 2016), including the exceptionally wet conditions around 1242 CE, align with major historical events such as the Mongol withdrawal from Hungary (Pinke et al. 2017; Büntgen and Cosmo 2016).

During the transition from the Medieval Climate Anomaly (MCA) to the Little Ice Age (LIA), an unusually hot and dry period was recorded in the first decade of the fourteenth century, particularly in 1306 and 1307 CE, which were also documented in central Europe and highlights the largest spatial coverage of this event (Bauch et al. 2020; Cook et al. 2024). This was followed by a slightly wetter phase during the Great Famine (1315–1317 CE), with 1315 CE standing out as the wettest year (SPI = 1.38), consistent with other central and eastern European records (Baek et al. 2020; Cook et al. 2015). Over the past 804 years, several distinct and long-lasting dry periods, known as megadroughts, have been observed during the intervals ~1340–1380, ~1400–1480, and ~1740–1800 CE (Ionita et al. 2021). The mid-fourteenth-century drought episodes overlap with the period of the Black Death (cc. 1347–1353 CE), contrasting with central Europe, where the climate was cold and wet (Büntgen et al. 2011a). Thus, these findings align with long-term drought reconstructions from eastern Europe, confirming the dry climate pattern during that period (Cook et al. 2024, 2015). The second major megadrought, occurring between 1452 and 1488 CE, coincided with the Spörer Minimum and, according to documentary evidence from eastern Europe, was marked by extremely cold winters and dry springs and summers (Table S1). Within this interval, the decade 1471–1480 CE ranks among the driest of the past millennium (Cook et al. 2022, 2015; Ionita et al. 2021). In 1453 CE, the year of the fall of Constantinople, a dry spring and famine were recorded, while drought conditions marked 1448–1451 CE. The years 1472 and 1474 CE were also extremely dry; the historical diaries indicate that in 1474 CE, the Danube could be crossed on foot (in Hungary), forest wildfires occurred, and in November, ripe cherries were harvested for the second time that year. The driest period of the past 804 years was 1701–1800 CE, with the distribution of extreme years showing a significant skewness (Fig. 5c). Notably, two long-lasting drought spells (1740–1780 and 1790–1803 CE) overlapped with the Dalton Minimum and are also clearly captured by independent hydroclimatic reconstructions from central and eastern Europe (Fig. 6) (Büntgen et al. 2011a; Nagavciuc et al. 2022a; Cook et al. 2020, 2024; Levanič et al. 2013; Wilson et al. 2005). The modern period began with extreme drought events, which included extreme dry years such as 1946 CE (−2.77), 1904 CE (−2.54), 1925 CE (−2.54), and 1928 CE (−2.07). The extreme years reported here correspond with the historical records of catastrophic events (Table S1).

The year 1660 CE was the driest year of the past 804 years (SPI = −3.07), with drought conditions documented across various parts of eastern Europe (Cook et al. 2015). The 1659–1660 CE drought caused severe famine across eastern Europe, with widespread crop failures. People reportedly consumed dried reeds, and anthropophagic cases were documented, illustrating the extreme societal impact of prolonged hydroclimatic stress (Cernovodeanu and Binder 1993). The 1585 CE drought, the second most severe in the current study (SPI = −2.91), affected a wide area of eastern Europe (Nagavciuc et al. 2022a; Cook et al. 2015, 2020) and was characterized by a dry spring and a barren summer. Springs, ponds, and pastures dried up; vegetation withered; and dust storms were widespread (Topor 1963; Cernovodeanu and Binder 1993; Teodoreanu 2017).

In the twentieth century, the driest year was 1946 CE (SPI = −2.77), which marked the last major famine associated with regional migration (Ionita et al. 2021; Nagavciuc et al. 2022a; Roibu et al. 2022; Ionita et al. 2025a, 2024; Nagavciuc et al. 2025). Nevertheless, this climate-induced famine was exacerbated by the economic and societal crisis after the Second World War. Historical sources have also been used to examine the wet years (especially during the extremely wet years). For example, 1229 CE recorded a very moist and cold spring and summer (SPI = 2.41), continuing from 1228 CE, with historical diaries describing famine and harvests rotting in the fields (Mihailescu 2004). Similarly, 1837 CE had a cold and extremely wet spring and summer (SPI = 2.60), with many heavy rainfall events

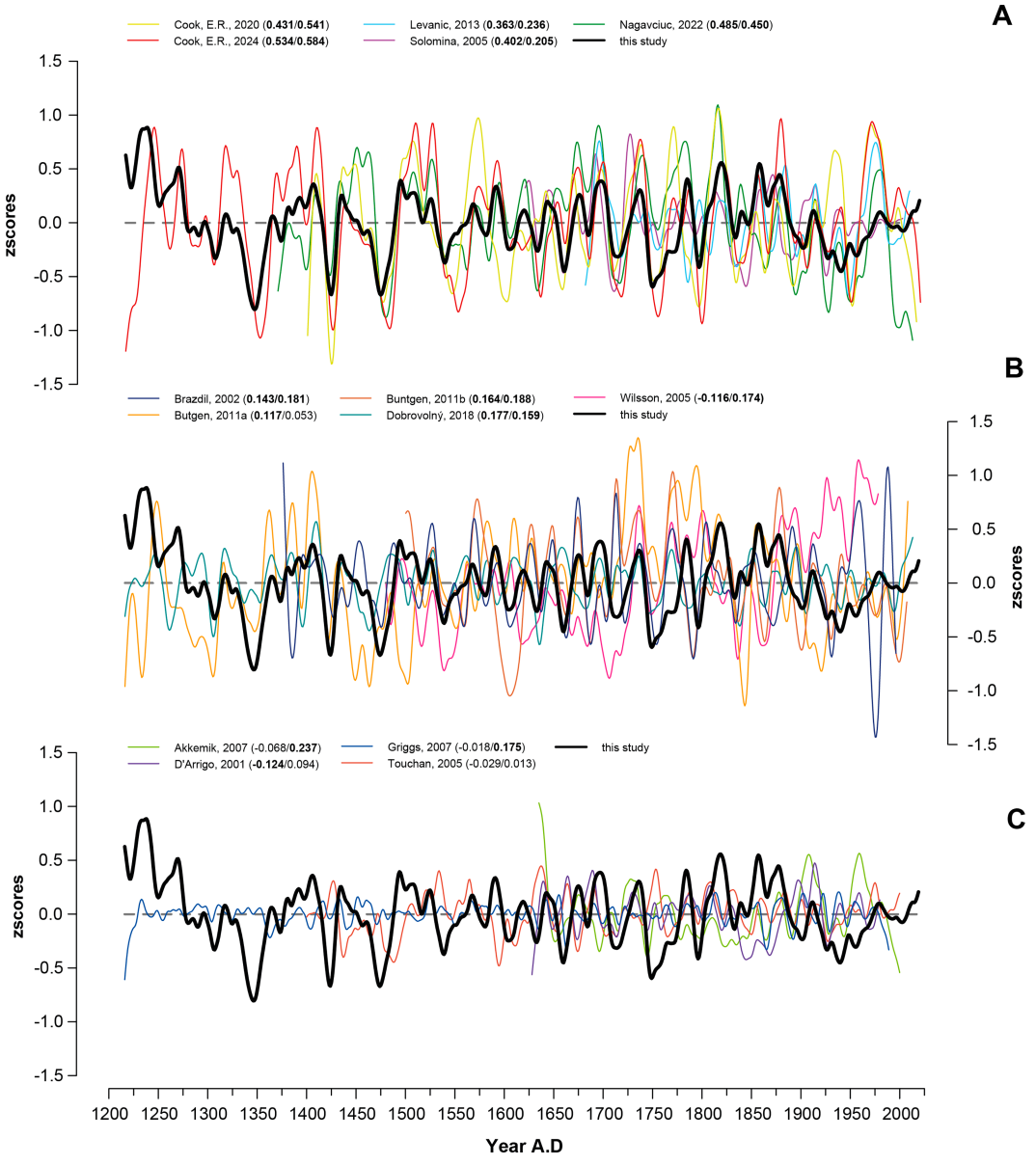

FIG. 6. Cross-regional comparison of hydroclimatic reconstructions from (a) eastern Europe, (b) central Europe, and (c) the Aegean region—all records are standardized (z scores) and smoothed with a 21-yr low-pass filter; correlation coefficients (r) are provided for both filtered and unfiltered values, with statistically significant values ($p < 0.05$) highlighted in bold.

leading to widespread flooding (Cernovodeanu and Binder 1993; Mihailescu 2004; Topor 1963). In 1813 CE, the entire summer was unusually wet and cold (SPI = 2.14), resulting in poor harvests and famine. Therefore, the reliability of this new hydroclimatic reconstruction is confirmed by the close correspondence between the extreme years identified in our record and historical evidence over the past ~800 years (Table S1).

Past hydroclimatic conditions in our analyzed region do not appear to have been affected by major volcanic eruptions. None of the nine largest, well-documented, and precisely dated historical eruptions (Toohey and Sigl 2017; Guillet et al. 2020; Esper et al. 2013) show a significant impact on the hydroclimate of eastern Europe. The absence of a postvolcanic signal in our reconstruction is consistent with similar findings from central Europe (Pauling et al. 2006) and may be explained by the limited sensitivity of oak ring widths to short-lived, externally forced perturbations in seasonal climate or by the broader spatial heterogeneity of precipitation responses to volcanic eruptions.

b. *Past climate and societal changes*

Climate has consistently influenced the evolution of human civilization, particularly in predominantly agrarian economies (Büntgen et al. 2011a; Xu et al. 2024; Pfister and Wanner 2021). In the preindustrial era, rapid demographic growth heightened

fears of famine, warfare, and plague pandemics, often linked to poor harvests caused by climatic anomalies. Such extreme events not only reduced crop yields but also intensified societal vulnerabilities, prompting unrest, migration waves, and the spread of disease (Cernovodeanu and Binder 1993; Ljungqvist et al. 2021; Xu et al. 2024; Kaniewski et al. 2025; Stothers 1999; Guillet et al. 2020). Rapid climatic shifts further drove large-scale entomo–zoological disruptions, including invasions of locusts, beetles, and rodents, which compounded food shortages and facilitated epidemic outbreaks, especially plague. The combined impact of these factors profoundly destabilized the biological and demographic equilibrium of affected populations, with catastrophic consequences. While direct evidence of the climate–society interaction in eastern Europe (especially the Lower Danubian territories) during this period is sparse, indirect evidence from surrounding regions (e.g., the Balkans, Hungary, or Russia) suggests significant disruptions in population and trade. In this context, our data provide valuable insights into how hydroclimatic variability influenced societal changes in preindustrial eastern Europe, revealing that wet or dry extremes often coincided with severe famines, regional migrations, and plague outbreaks, further aggravated by wars, Mongol invasions, and political instability. For instance, climatic conditions marked both the advance and the retreat of the Mongols in Europe (Yue et al. 2026; Büntgen and Cosmo 2016). During the drought event in 1223 CE, the Mongols' first appearance on the Kalka River (Ukraine) was recorded, and the victory at the homonymous battle (31 May 1223 CE) marked the start of their westward expansion (Gabriel 2006; Jackson 2018). In that year, the Dnieper River could be crossed "by dry land," and widespread forest fires burned across the region (Mihailescu 2004). In contrast, their controversial sudden retreat from Hungary in 1242 CE has been linked to wet conditions (Büntgen and Cosmo 2016; Pinke et al. 2017). The Great Famine of 1315–1317 CE, triggered by an exceptionally wet period across Europe, led to widespread starvation and increased mortality, a pattern that recurred during subsequent climate-related famines in the region, such as those in 1596–1597 and 1691–1692 CE, which have been linked to periods of extreme drought and cold (Ljungqvist et al. 2024). Some regional rulers even received nicknames inspired by those harsh times—for example, Ștefăniă Vodă, called "Reed Vodă," referring to the severe drought of 1659–1660 CE when, according to chronicles, people survived by eating dried reed (Cernovodeanu and Binder 1993). The region's most recent large-scale famine in 1946–47 CE, exacerbated by postwar policies, was triggered by a severe drought, prompting significant regional migration (Ionescu and Ionescu 2006; Ionita et al. 2025a).

c. *European context of the new drought reconstructions*

To evaluate the robustness of our hydroclimatic reconstruction, we compared it with precipitation- and drought-sensitive proxy records from eastern Europe, central Europe, and the Aegean (Fig. 6). Statistically significant positive correlations ($p < 0.05$) were obtained with five high-resolution reconstructions from eastern Europe, with values ranging from 0.21 to 0.58 in the raw series and from 0.40 to 0.53 after 21-yr smoothing. The reconstruction reliably captures significant decadal variability documented in published eastern European datasets (Cook et al. 2020, 2024; Solomina et al. 2005; Levanič et al. 2013; Nagavciuc et al. 2022a), though some amplitude and timing differences are evident, especially before 1500 CE. In contrast, comparisons with central European and Aegean records revealed a shift in correlation, from weakly positive to negative values, in both smoothed and unsmoothed data. In central Europe, our reconstruction shares broad variability with existing datasets (Büntgen et al. 2011a,b; Dobrovolný et al. 2018a, manuscript submitted to *Climate Past*; Brázdil et al. 2002; Wilson et al. 2005), with evident synchronicity of wet and dry anomalies after ~1600 CE, but correlation coefficients remain low or negative. Similarly, in the Aegean, agreement among reconstructions is generally weaker, reflecting spatial heterogeneity and differences in proxy sensitivity, though our reconstruction aligns reasonably well with previously published datasets, particularly for the period after 1800 CE (Akkemik et al. 2005; Touchan et al. 2005; D'Arrigo and Cullen 2001; Griggs et al. 2007). This pattern likely reflects the shared influence of continental-scale climate drivers and regional land–atmosphere feedback, which coherently modulate hydroclimatic variability over eastern Europe. In contrast, the shift to negative, statistically significant correlations with central European and Aegean reconstructions suggests distinct drought regimes, possibly shaped by distinct atmospheric circulation patterns. These divergent climatic controls result in asynchronous drought expressions across regions, explaining the contrasting correlation structures. Moreover, these differences also reflect how the individual reconstructions were produced (Table S2). Most records are based on tree-ring width but use different species (e.g., oak, silver fir, black pine, or mixed-species networks). These species do not respond to climate in the same way. Some are more sensitive to moisture stress, others are more sensitive to temperature, and their strongest response does not always occur at the same time during the growing season. Nagavciuc et al. (2022a) used a different approach, reconstructing hydroclimate from stable-isotope ratios in tree-ring cellulose. Unlike ring width, $\delta^{18}O$ is controlled by isotopic processes related to source water and evaporation. This means the climatic signal is integrated through a different physiological pathway and may highlight somewhat different aspects of moisture variability. There are also differences in what was reconstructed. Some studies focus on precipitation (as raw data), while others use drought indices such as SPI, SPEI, self-calibrating PDSI (scPDSI), or the Z index. These indices combine temperature and precipitation in different ways and operate on different time scales. They are related but not interchangeable. In addition, the seasonal windows differ across studies, with some reconstructions targeting early growing season conditions (March–June) and others focusing on summer months (June–August). As a result, each record samples a slightly different part of the climate signal. All these differences should be kept in mind when interpreting the correlation patterns presented in this study, particularly the contrast between eastern European and central European or Aegean records.

d. *Large-scale drivers of hydroclimate in the eastern part of Europe*

In the following subsection, we analyze the large-scale atmospheric circulation patterns associated with extreme hydroclimatic

variations. The focus is on high (SPI12 July > 1) and low (SPI12 July < -1) years. In this respect, we employ the composite map analysis (see data and methods section, large-scale atmospheric circulation description), a statistical approach used to reveal statistically robust and recurring circulation features associated with extreme events. The composite maps with the Z500 cover the period 1836–2015, while the composite maps with the SST cover the period 1854–2019. Large-scale circulation modulates the near-surface temperature and precipitation and thus drought. Persistent anticyclones/atmospheric blocking amplify subsidence, clear skies, and warm–dry advection, fostering heat waves, soil moisture depletion, and drought from regional to continental scales (Bakke et al. 2023; Ionita et al. 2022; Kingston et al. 2015; Nagavciuc et al. 2024). For instance, in regions affected by descending air masses (high pressure systems), such as subtropical zones, droughts occur more often due to the associated warming and drying of the air and the lack of precipitation. Our results indicate that wet and dry extreme years over eastern Europe, as measured by SPI12, are strongly associated with distinct patterns in atmospheric circulation and SST anomalies. High SPI12 years—indicative of wetter conditions—correspond to a pronounced negative Z500 centered over the central and eastern part of Europe, extending up the central North Atlantic basin and a high pressure center over the Arctic region and Eurasia (Fig. 7a). Conversely, low SPI12 years (drier conditions) are associated with a positive geopotential height anomaly over the central and eastern part of Europe and a negative center of Z500 anomalies over Greenland extending into the northern part of the North Atlantic basin (Fig. 7b). During wet years, atmospheric blocking is often displaced northwestward relative to southeastern Europe, with increased blocking activity upstream and reduced blocking locally. This shift helps disrupt persistent anticyclonic regimes—conditions typically associated with extended droughts and heat waves—and instead promotes cyclonic flow and increased precipitation over eastern Europe. In contrast, dry years are associated with a high pressure center dominating eastern and central Europe. This enhances the frequency of atmospheric blocking locally (Ionita et al. 2025b; Kautz et al. 2022), which deflects storm tracks northward and suppresses local precipitation, resulting in prolonged moisture deficits and negative SPI12 values, manifesting as drought conditions (Fig. 7b). These findings are supported by earlier research demonstrating the critical role of atmospheric blocking in shaping European hydroclimate extremes (Ionita et al. 2021; Laaha et al. 2017; Kingston et al. 2015).

To assess whether our composite map results might instead reflect general dynamical consistency rather than reanalysis-specific uncertainty behavior, we also considered comparisons to independent, proxy-constrained products spanning the last millennium. In particular, we performed a similar analysis on the ensemble Kalman fitting paleo-reanalysis (Franke et al. 2017), which provides spatially explicit reconstructions of Z500 over the period 1605–2005 and is independent of the 20CR observing network. The composite maps for Z500 (Fig. S5) yield patterns that are essentially indistinguishable from the 20CR-based results. This motivates the view that, while the early 20CR variance collapse can affect absolute uncertainty estimates, the qualitative conclusions are robust when evaluated against long proxy reconstructions.

In addition to atmospheric drivers, the state of the Atlantic Ocean exerts a significant impact on hydroclimatic anomalies across Europe (Ionita et al. 2022). The composite SST maps (Figs. 7c,d) reveal that wet (dry) years are marked by warm (cold) SST anomalies across large stretches of the subtropical and tropical Atlantic basin, along with cold (warm) anomalies along the east coast of the United States. These SST patterns are also evident in parts of the South Atlantic and sections of the Indian Ocean during wet (dry) periods. This relationship is consistent with the broader literature, which has established robust links between Atlantic and Mediterranean SST variability and European hydroclimate on interannual-to-decadal time scales (Feudale and Shukla 2011; Kingston et al. 2015; Ionita et al. 2021; Laaha et al. 2017; Ionita et al. 2022).

Recent dendrochronological studies further corroborate these associations, demonstrating that tree-ring records across Europe are sensitive to SST-driven hydroclimate variability (Nagavciuc et al. 2019a; Roibu et al. 2022; Nagavciuc et al. 2020). The emerging picture confirms that both large-scale atmospheric patterns (high and low pressure systems) and oceanic conditions (SST anomalies) act synergistically to modulate the occurrence and duration of extreme precipitation events and droughts in eastern Europe. The results emphasize the need to consider both atmospheric and SST variability in predicting and managing drought and flood risk for the region.

5. Outlook: From past droughts to future risks

Advanced climate models suggest a significant reduction in future Mediterranean precipitation (IPCC 2021), and some observational studies also report a current decline, often attributing it to human influence (IPCC 2021; Balting et al. 2021). However, in a recent paper, Vicente-Serrano et al. (2025) showed that strong natural variability of precipitation in Mediterranean region (e.g., Spain, Italy, Greece, Cyprus, southern France) and the eastern part of Europe (e.g., Romania, Turkey, Bulgaria, Hungary, and Moldova) is driven mainly by the large-scale atmospheric circulation, and there is negligible evidence of long-term change. Moreover, Mediterranean precipitation has remained nearly unchanged, with observed trends in specific periods and subregions primarily attributed to internal atmospheric variability. Our reconstruction over the past 804 years shows no statistically significant long-term trend in July SPI12, suggesting that the reconstructed hydroclimate variability is dominated by interannual-to-multidecadal fluctuations within the limits of this TRW-based reconstruction and its instrumental calibration period. To catch a glimpse of the future, we have extended our analysis until the end of the twenty-first century by considering the July SPI12 average over Romania, based on bias-corrected Coordinated Regional Climate Downscaling Experiment (CORDEX) data over Romania, specifically the Romanian Climate Library (RoCLIB) dataset (Dumitrescu et al. 2023). Ten regional climate models, provided by the European CORDEX (EURO-CORDEX) initiative (Jacob et al. 2014), were adjusted using as a reference the Romanian Climatic Dataset (ROCADA) gridded dataset (Dumitrescu and Birsan 2015), which is based on temperature data from 150 stations and precipitation from 188 stations with at least 30% completeness of records over 1961–2013 used for

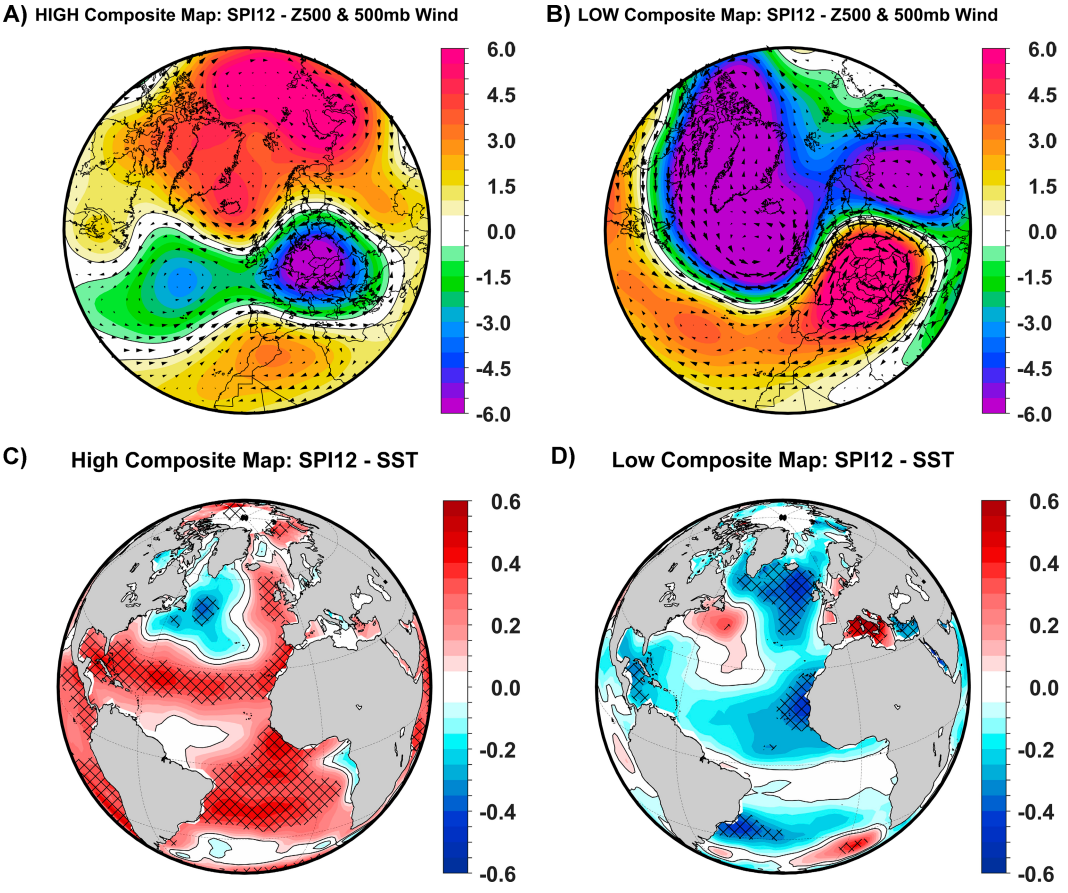

FIG. 7. (a) The composite map between wet years (July SPI12 > 1 std dev) and annual Z500 and 500-mb wind; (b) the composite map between dry years (July SPI12 < 1 std dev) and annual Z500 and 500-mb wind; (c) the composite map between wet years (July SPI12 > 1 std dev) and annual SST; and (d) the composite map between dry years (July SPI12 < 1 std dev) and annual SST. Analyzed period: (a),(b) 1835–2015 and (c),(d) 1854–2019. Units: standardized anomalies. The hatching highlights significant values at a confidence level of 95%, based on a double Student's *t* test. In (a)–(d), the annual data are computed as the annual mean for Z500 and SST from August (previous year) to July (current year).

building a 0.1° × 0.1° resolution grid covering the entire national territory of Romania. Two RCP climate projections were selected: a moderate (radiative forcing to stabilize at 4.5 W m^{-2} before the year 2100) and a higher one (radiative forcing to stabilize at 8.5 W m^{-2} before the year 2100). A list of the models used in the RoCLIB dataset is provided in Table 1 of Dumitrescu et al. (2023). Figure 8 illustrates both the historical reconstruction of SPI12 for July (1221–2019, black line) and historical ensemble mean and future projections (1972–2100, red line for model mean, with pink shading indicating uncertainty bands) under two greenhouse gas scenarios: RCP4.5 (Fig. 8a) and RCP8.5 (Fig. 8b). Across the full CORDEX models ensemble mean, some similar patterns emerge for Romania (Fig. 8). As previously mentioned, the historical record reveals interannual and multidecadal variability, with the July SPI12 fluctuating between wet and dry periods but lacking an evident long-term trend. This pattern is retained in the projected period, where the ensemble mean remains close to the historical mean, suggesting an absence of a statistically robust trend toward increased drought frequency or intensity throughout the twenty-first century, for both RCP4.5 and RCP8.5 scenarios. Notably, while year-to-year variability continues, the model consensus does not support an intensification of annual drought conditions in Romania, implying continuity rather than escalation of present patterns. While the temporal correlation between the observed July SPI12 and the CORDEX-based ensemble mean is modest ($r = 0.25$), the models exhibit a relatively high skill in reproducing the statistical properties and extreme tails of the historical distribution. Over the 1972–2005 overlapping period, the ensemble mean captures the full range of observed hydroclimatic variability, with a minimum value of −0.96 that closely matches the observed extreme of −0.90. Overall, the ensemble mean shows a slightly higher standard deviation ($\sigma = 0.80$) compared to the observations ($\sigma = 0.38$), indicating that the regional climate models are sensitive to the high interannual variability characteristic of the Romanian climate. The physical basis for this variability in the models might be linked to the simulation of large-scale atmospheric circulation and SST forcing, which drive the moisture flux into eastern Europe.

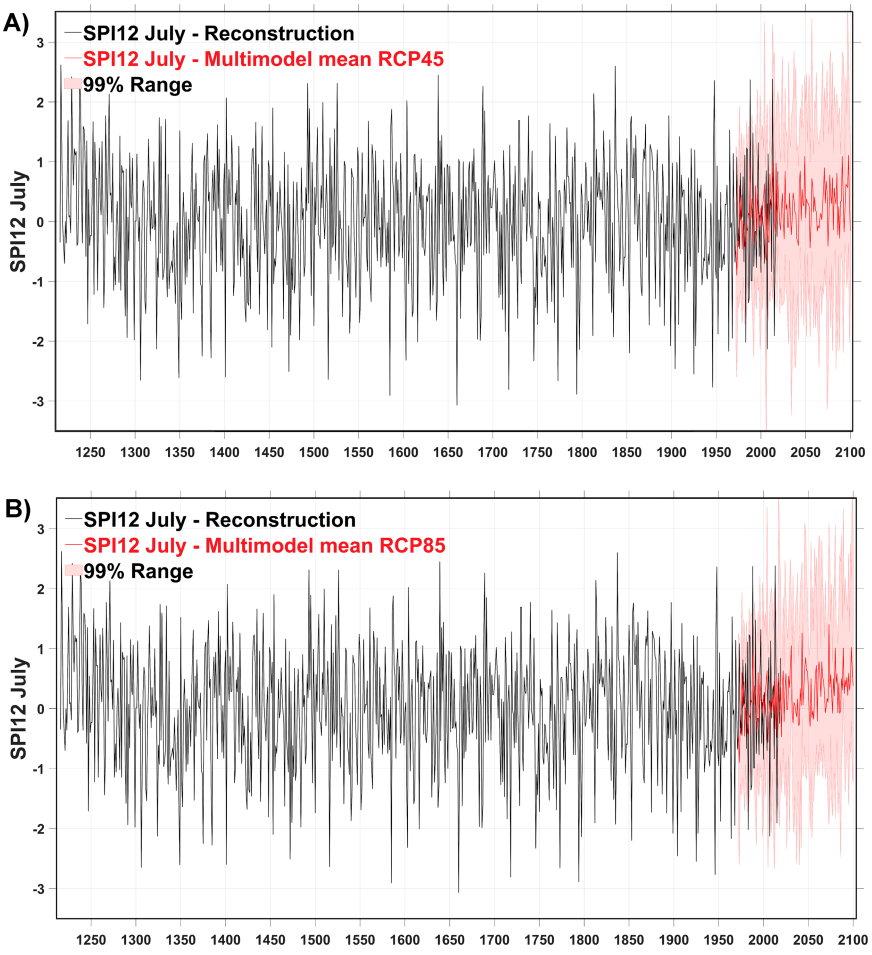

FIG. 8. Future drought projections. CORDEX simulated July SPI12 calculated using the monthly precipitation values, averaged over Romania, over the period 1972–2100. The black line indicates the SPI12 July reconstruction, the red thick lines represent the ensemble mean of the 10 models used in this study, and the pink shading around the model mean shows the two-tailed 99% range estimated from individual ensemble members. (a) Future estimation based on RCP4.5; (b) as in (a), but for RCP8.5.

The consistency in the magnitude of extremes between the reconstruction and the models provides confidence that the future projections are grounded in a realistic representation of regional climate dynamics, as suggested by Vicente-Serrano et al. (2025).

However, the projection period is characterized by a highlighted expansion of uncertainty. The pink shading around the red line, representing the 99% range of ensemble spread, grows substantially wider after 2006, being especially pronounced under the RCP8.5 scenario. This expanding envelope of uncertainty reflects a growing divergence in model responses to future greenhouse gas forcing, as well as the compounding of uncertainties related to emissions pathways, regional climate sensitivities, and hydrological feedback in a warming climate. The result is an uncertainty range for future hydroclimatic conditions that not only encompasses but also sometimes exceeds the most extreme historical episodes. This broadening of potential outcomes reflects the inherent unpredictability associated with regional climate projections under high-emission scenarios, underscoring the critical role of emission pathways in determining the magnitude of both mean changes and risks of extreme events. While the ensemble mean is inherently smoother than our reconstruction, individual CORDEX members successfully replicate the full range of historical SPI12 extremes (reaching values below −3.0 and higher than 3.0), with an intermodel spread that expands by approximately 60% by 2100 under RCP8.5, reflecting a significant widening of potential hydroclimatic outcome. The limited trend in the ensemble means, coupled with high interannual variability and widening uncertainty, closely mirrors the findings of Vicente-Serrano et al. (2025), who demonstrated that for the broader Mediterranean region, high temporal variability dominates over any detectable long-term trend in precipitation. Their study provides robust observational evidence that precipitation regimes across the Mediterranean have mainly remained stable since the late nineteenth century, with large fluctuations mostly attributable to atmospheric circulation patterns

rather than anthropogenic climate forcing. The present results for Romania suggest a similar regime: While climate models project large uncertainty bands suggesting the potential for more extreme droughts, the central tendency of those projections does not deviate substantially from the established historical variability. In summary, the CORDEX-based, bias-corrected projections suggest that Romania's drought risk under climate change scenarios may not substantially deviate from historical patterns of the past millennium, but the range of possible futures expands considerably, especially under high-emission scenarios. This emphasizes adaptation strategies that can accommodate a widening spectrum of extremes rather than a simple shift in mean drought frequency or severity, in agreement with observational and modeling evidence for the Mediterranean region.

6. Conclusions

We present a new, well-replicated oak chronology from eastern Europe and a statistically robust reconstruction of annual hydroclimate back to 1221 CE. The chronology meets the reliability standards and captures a stable regional drought signal across Romania, Moldova, and Ukraine, making it suitable for paleoclimatic inference. The reconstruction reveals pronounced interannual-to-multidecadal variability, with several megadroughts—especially in the fourteenth, fifteenth, and eighteenth centuries, that align with historical evidence of societal stress. Although these periods coincide and suggest heightened vulnerability, they do not by themselves demonstrate causality, highlighting that human impacts were strongly mediated by political and economic conditions.

Mechanistic analyses link hydroclimatic extremes over the eastern Europe to large-scale atmospheric circulation and North Atlantic SST anomalies. Forward-looking simulations based on bias-corrected EURO-CORDEX projections suggest that mean hydroclimatic conditions may remain relatively stable; however, the variability envelope is expected to widen substantially under both moderate and high forcing scenarios. This implies a future characterized less by a shift in the mean state and more by the amplification of extremes.

Although our reconstruction indicates no significant long-term trend in precipitation variability, and regional projections similarly lack a robust precipitation signal associated with climate warming, we emphasize that the use of a precipitation-based drought index (SPI) does not account for temperature-driven increases in atmospheric evaporative demand. Consequently, ongoing warming could intensify drought risk even in the absence of declining precipitation.

In summary, this study quantifies the amplitude and persistence of natural hydroclimatic variability in eastern Europe, identifies the circulation and oceanic drivers of extreme summers, and positions these within a long-term sociohistorical context. Extending across more than eight centuries, the reconstruction sheds new light on the interplay between climate variability and human vulnerability in a region shaped by complex political and economic transformations. These findings emphasize that drought risk in eastern Europe (past, present, and future) is dominated by internal climate dynamics, and they highlight the need for adaptive water management and resilience strategies that account for growing variability and the persistence of extremes.

Acknowledgments. This work was supported by a grant of the Ministry of Research, Innovation and Digitization, under the "Romania's National Recovery and Resilience Plan—Founded by EU–NextGenerationEU" program, project "Compound extreme events from a long-term perspective and their impact on forest growth dynamics (CExForD)" 760074/23.05.2023, code 287/30.11.2022, within Pillar III, Component C9, Investment 8. T. W. was supported by the National Science Center, Poland, Project 2016/22/A/HS3/00285. C. C. R., V. N. and M. I. designed the study and methodology, analyzed the data, and wrote the article draft; C. P. and T. W. helped write the original draft, interpreted the results, and reviewed. C. M. A. and M. I. S. realized the historical investigation. All the authors contributed critically to the drafts and gave their final acceptance for publication. The authors declare no competing interests.

Data availability statement. The annual July SPI12 reconstruction for the period 1221–2019 can be downloaded from https://doi.org/10.5281/zenodo.19709534.

REFERENCES

Abrams, M. D., 1990: Adaptations and responses to drought in *Quercus* species of North America. *Tree Physiol.*, **7**, 227–238, https://doi.org/10.1093/treephys/7.1-2-3-4.227.

Akkemik, Ü., N. Dağdeviren, and A. Aras, 2005: A preliminary reconstruction (A.D. 1635–2000) of spring precipitation using oak tree rings in the western Black Sea region of Turkey. *Int. J. Biometeor.*, **49**, 297–302, https://doi.org/10.1007/s00484-004-0249-8.

Allen, M. F., 2015: How oaks respond to water limitation. *Proceedings of the Seventh California Oak Symposium: Managing Oak Woodlands in a Dynamic World*, Department of Agriculture, Forest Service, Pacific Southwest Research Station, General Tech. Rep. PSW-GTR-251, 13–22, https://research.fs.usda.gov/treesearch/49910.

Anders, I., J. Stagl, I. Auer, and D. Pavlik, 2013: Climate change in central and eastern Europe. *Managing Protected Areas in Central and Eastern Europe under Climate Change*, S. Rannow and M. Neubert, Eds., Springer, 17–30, https://doi.org/10.1007/978-94-007-7960-0_2.

Árvai, M., A. Morgós, and Z. Kern, 2018: Growth-climate relations and the enhancement of drought signals in pedunculate oak (*Quercus robur* L.) tree-ring chronology in Eastern Hungary. *iForest*, **11**, 267–274, https://doi.org/10.3832/ifor2348-011.

Atwell, W. S., 2001: Volcanism and short-term climatic change in East Asian and world history, c. 1200-1699. *J. World Hist.*, **12**, 29–98, https://doi.org/10.1353/jwh.2001.0002.

Baek, S. H., and Coauthors, 2020: A quantitative hydroclimatic context for the European Great Famine of 1315–1317. *Commun. Earth Environ.*, **1**, 19, https://doi.org/10.1038/s43247-020-00016-3.

Bakke, S. J., M. Ionita, and L. M. Tallaksen, 2023: Recent European drying and its link to prevailing large-scale atmospheric patterns. *Sci. Rep.*, **13**, 21921, https://doi.org/10.1038/s41598-023-48861-4.

Balting, D. F., A. AghaKouchak, G. Lohmann, and M. Ionita, 2021: Northern Hemisphere drought risk in a warming climate. *npj Climate Atmos. Sci.*, **4**, 61, https://doi.org/10.1038/s41612-021-00218-2.

Bauch, M., T. Labbé, A. Engel, and P. Seifert, 2020: A prequel to the Dantean Anomaly: The precipitation seesaw and droughts of 1302 to 1307 in Europe. *Climate Past*, **16**, 2343–2358, https://doi.org/10.5194/cp-16-2343-2020.

Bose, A. K., and Coauthors, 2021: Climate sensitivity and drought seasonality determine post-drought growth recovery of *Quercus petraea* and *Quercus robur* in Europe. *Sci. Total Environ.*, **784**, 147222, https://doi.org/10.1016/j.scitotenv.2021.147222.

Brázdil, R., P. Stepánková, T. Kyncl, and J. Kyncl, 2002: Fir tree-ring reconstruction of March–July precipitation in southern Moravia (Czech Republic), 1376-1996. *Climate Res.*, **20**, 223–239, https://doi.org/10.3354/cr020223.

——, P. Dobrovolný, J. Luterbacher, A. Moberg, C. Pfister, D. Wheeler, and E. Zorita, 2010: European climate of the past 500 years: New challenges for historical climatology. *Climatic Change*, **101**, 7–40, https://doi.org/10.1007/s10584-009-9783-z.

——, ——, M. Trnka, O. Kotyza, L. Řezníčková, H. Valášek, P. Zahradníček, and P. Štěpánek, 2013: Droughts in the Czech Lands, 1090–2012 AD. *Climate Past*, **9**, 1985–2002, https://doi.org/10.5194/cp-9-1985-2013.

——, ——, J. Mikšovský, P. Pišoft, M. Trnka, M. Možný, and J. Balek, 2022: Documentary-based climate reconstructions in the Czech Lands 1501–2020 CE and their European context. *Climate Past*, **18**, 935–959, https://doi.org/10.5194/cp-18-935-2022.

Briffa, K. R., P. D. Jones, T. M. L. Wigley, J. R. Pilcher, and M. G. L. Baillie, 1983: Climate reconstruction from tree rings: Part 1, basic methodology and preliminary results for England. *J. Climatol.*, **3**, 233–242, https://doi.org/10.1002/joc.3370030303.

——, ——, T. S. Bartholin, D. Eckstein, F. H. Schweingruber, W. Karlén, P. Zetterberg, and M. Eronen, 1992: Fennoscandian summers from AD 500: Temperature changes on short and long timescales. *Climate Dyn.*, **7**, 111–119, https://doi.org/10.1007/BF00211153.

Büntgen, U., and N. Di Cosmo, 2016: Climatic and environmental aspects of the Mongol withdrawal from Hungary in 1242 CE. *Sci. Rep.*, **6**, 25606, https://doi.org/10.1038/srep25606.

——, and Coauthors, 2011a: 2500 years of European climate variability and human susceptibility. *Science*, **331**, 578–582, https://doi.org/10.1126/science.1197175.

——, R. Brázdil, P. Dobrovolný, M. Trnka, and T. Kyncl, 2011b: Five centuries of Southern Moravian drought variations revealed from living and historic tree rings. *Theor. Appl. Climatol.*, **105**, 167–180, https://doi.org/10.1007/s00704-010-0381-9.

Cernovodeanu, P., and P. Binder, 1993: *Cavalerii Apocalipsului: Calamităi Naturale Din Trecutul României (Până la 1800).* Editura Silex, 255 pp.

Compo, G. P., J. S. Whitaker, and P. D. Sardeshmukh, 2006: Feasibility of a 100-Year reanalysis using only surface pressure data. *Bull. Amer. Meteor. Soc.*, **87**, 175–190, https://doi.org/10.1175/BAMS-87-2-175.

——, and Coauthors, 2011: The twentieth century reanalysis project. *Quart. J. Roy. Meteor. Soc.*, **137**, 1–28, https://doi.org/10.1002/qj.776.

Constantin, C., 2015: Romanian grain market in the British Russophobia context (1829–1853). *Hiperboreea J.*, **2**, 95–107, https://doi.org/10.3406/hiper.2015.886.

Cook, B. I., and Coauthors, 2022: Megadroughts in the Common Era and the Anthropocene. *Nat. Rev. Earth Environ.*, **3**, 741–757, https://doi.org/10.1038/s43017-022-00329-1.

——, E. R. Cook, K. J. Anchukaitis, and D. Singh, 2024: Characterizing the 2010 Russian heat wave–Pakistan flood concurrent extreme over the last millennium using the Great Eurasian Drought Atlas. *J. Climate*, **37**, 4389–4401, https://doi.org/10.1175/JCLI-D-23-0773.1.

Cook, E. R., and L. A. Kairiukstis, 1990: *Methods of Dendrochronology: Applications in the Environmental Sciences.* Kluwer, 304 pp.

——, and Coauthors, 2015: Old World megadroughts and Pluvials during the Common Era. *Sci. Adv.*, **1**, e1500561, https://doi.org/10.1126/sciadv.1500561.

——, and Coauthors, 2020: The European Russia Drought Atlas (1400–2016 CE). *Climate Dyn.*, **54**, 2317–2335, https://doi.org/10.1007/s00382-019-05115-2.

Coumou, D., and S. Rahmstorf, 2012: A decade of weather extremes. *Nat. Climate Change*, **2**, 491–496, https://doi.org/10.1038/nclimate1452.

Cufar, K., M. Grabner, A. Morgós, E. M. del Castillo, M. Merela, and M. de Luis, 2014: Common climatic signals affecting oak tree-ring growth in SE Central Europe. *Trees*, **28**, 1267–1277, https://doi.org/10.1007/s00468-013-0972-z.

D'Arrigo, R., and H. M. Cullen, 2001: A 350-year (AD 1628–1980) reconstruction of Turkish precipitation. *Dendrochronologia*, **19**, 169–177.

Dobrovolný, P., and Coauthors, 2010: Monthly, seasonal and annual temperature reconstructions for Central Europe derived from documentary evidence and instrumental records since AD 1500. *Climatic Change*, **101**, 69–107, https://doi.org/10.1007/s10584-009-9724-x.

——, R. Brázdil, M. Trnka, M. Rybníček, T. Kolář, M. Možný, T. Kyncl, and U. Büntgen, 2018a: A 500-year multi-proxy drought reconstruction for the Czech Lands. *Climate Past Discuss*, https://doi.org/10.5194/cp-2018-160.

——, M. Rybníček, T. Kolář, R. Brázdil, M. Trnka, and U. Büntgen, 2018b: May–July precipitation reconstruction from oak tree-rings for Bohemia (Czech Republic) since AD 1040. *Int. J. Climatol.*, **38**, 1910–1924, https://doi.org/10.1002/joc.5305.

Drobyshev, I., M. Niklasson, O. Eggertsson, H. Linderson, and K. Sonesson, 2008: Influence of annual weather on growth of pedunculate oak in southern Sweden. *Ann. For. Sci.*, **65**, 512, https://doi.org/10.1051/forest:2008033.

Dudaș, F., 1999: *Catastrofe naturale în Transilvania, În lumina ănsemnărilor scrise pe cările românești vechi între anii 1500 și 1900.* Editura de Vest, 176 pp.

Dumitrescu, A., and M.-V. V. Birsan, 2015: ROCADA: A gridded daily climatic dataset over Romania (1961–2013) for nine meteorological variables. *Nat. Hazards*, **78**, 1045–1063, https://doi.org/10.1007/s11069-015-1757-z.

——, V.-A. Amihaesei, and S. Cheval, 2023: RoCliB– bias-corrected CORDEX RCMdataset over Romania. *Geosci. Data J.*, **10**, 262–275, https://doi.org/10.1002/gdj3.161.

Durbin, J., and G. S. Watson, 1950: Testing for serial correlation in least squares regression. I. *Biometrika*, **37**, 409–428, https://doi.org/10.2307/2332391.

Ellenberg, H. H., 2009: *Vegetation Ecology of Central Europe.* Cambridge University Press, 756 pp.

Esper, J., E. Cook, P. Krusic, K. Peters, and F. Schweingruber, 2003: Tests of the RCS method for preserving low-frequency variability in long tree-ring chronologies. *Tree Ring Res.*, **59**, 81–98.

——, D. C. Frank, R. J. S. Wilson, and K. R. Briffa, 2005: Effect of scaling and regression on reconstructed temperature amplitude for the past millennium. *Geophys. Res. Lett.*, **32**, L07711, https://doi.org/10.1029/2004gl021236.

——, L. Schneider, P. J. Krusic, J. Luterbacher, U. Büntgen, M. Timonen, F. Sirocko, and E. Zorita, 2013: European summer temperature response to annually dated volcanic eruptions

over the past nine centuries. *Bull. Volcanol.*, **75**, 736, https://doi.org/10.1007/s00445-013-0736-z.

——, and Coauthors, 2016: Ranking of tree-ring based temperature reconstructions of the past millennium. *Quat. Sci. Rev.*, **145**, 134–151, https://doi.org/10.1016/j.quascirev.2016.05.009.

Feudale, L., and J. Shukla, 2011: Influence of sea surface temperature on the European heat wave of 2003 summer. Part II: A modeling study. *Climate Dyn.*, **36**, 1705–1715, https://doi.org/10.1007/s00382-010-0789-z.

Feuillat, F., J.-L. Dupouey, D. Sciama, and R. Keller, 1997: A new attempt at discrimination between *Quercus petraea* and *Quercus robur* based on wood anatomy. *Can. J. For. Res.*, **27**, 343–351, https://doi.org/10.1139/x96-174.

Fischer, E. M., J. Luterbacher, E. Zorita, S. F. B. Tett, C. Casty, and H. Wanner, 2007: European climate response to tropical volcanic eruptions over the last half millennium. *Geophys. Res. Lett.*, **34**, L05707, https://doi.org/10.1029/2006GL027992.

Fonti, P., and I. García-González, 2008: Earlywood vessel size of oak as a potential proxy for spring precipitation in mesic sites. *J. Biogeogr.*, **35**, 2249–2257, https://doi.org/10.1111/j.1365-2699.2008.01961.x.

Frank, D., J. Esper, and E. R. Cook, 2007: Adjustment for proxy number and coherence in a large-scale temperature reconstruction. *Geophys. Res. Lett.*, **34**, L16709, https://doi.org/10.1029/2007GL030571.

Franke, J., S. Brönnimann, J. Bhend, and Y. Brugnara, 2017: A monthly global paleo-reanalysis of the atmosphere from 1600 to 2005 for studying past climatic variations. *Sci. Data*, **4**, 170076, https://doi.org/10.1038/sdata.2017.76.

Friedrichs, D. A., U. Bntgen, D. C. Frank, J. Esper, B. Neuwirth, and J. Loffler, 2009: Complex climate controls on 20th century oak growth in Central-West Germany. *Tree Physiol.*, **29**, 39–51, https://doi.org/10.1093/treephys/tpn003.

Fritts, H. C., 1976: *Tree Rings and Climate.* Academic Press, 567 pp.

Früchtenicht, E., J. Bock, V. Feucht, and W. Brüggemann, 2021: Reactions of three European oak species (*Q. robur*, *Q. petraea* and *Q. ilex*) to repetitive summer drought in sandy soil. *Trees For. People*, **5**, 100093, https://doi.org/10.1016/j.tfp.2021.100093.

Gabriel, R. A., 2006: *Genghis Khan's Greatest General: Subotai the Valiant.* University of Oklahoma Press, 176 pp.

Geacu, S., and I. Grigorescu, 2022: Historical changes in urban and peri-urban forests: Evidence from the Galai Area, Romania. *Land*, **11**, 2043, https://doi.org/10.3390/land11112043.

Giurescu, C. C., 1976: *Istoria pădurii românești din cele mai vechi timpuri pînă astazi.* Editura Ceres, 394 pp.

Griggs, C., A. DeGaetano, P. Kuniholm, and M. Newton, 2007: A regional high-frequency reconstruction of May–June precipitation in the north Aegean from oak tree rings, A.D. 1089–1989. *Int. J. Climatol.*, **27**, 1075–1089, https://doi.org/10.1002/joc.1459.

Guillet, S., C. Corona, F. Ludlow, C. Oppenheimer, and M. Stoffel, 2020: Climatic and societal impacts of a "forgotten" cluster of volcanic eruptions in 1108-1110 CE. *Sci. Rep.*, **10**, 6715, https://doi.org/10.1038/s41598-020-63339-3.

Haldon, J., L. Mordechai, T. P. Newfield, A. F. Chase, A. Izdebski, P. Guzowski, I. Labuhn, and N. Roberts, 2018: History meets palaeoscience: Consilience and collaboration in studying past societal responses to environmental change. *Proc. Natl. Acad. Sci. USA*, **115**, 3210–3218, https://doi.org/10.1073/pnas.1716912115.

Harris, I., T. J. Osborn, P. Jones, and D. Lister, 2020: Version 4 of the CRU TS monthly high-resolution gridded multivariate climate dataset. *Sci. Data*, **7**, 109, https://doi.org/10.1038/s41597-020-0453-3.

Homfeld, I. K., U. Büntgen, F. Reinig, M. C. A. Torbenson, and J. Esper, 2024: Application of RCS and signal-free RCS to tree-ring width and maximum latewood density data. *Dendrochronologia*, **85**, 126205, https://doi.org/10.1016/j.dendro.2024.126205.

Horeanu, C., 1996: *Dendrologie.* Curs litografiat, Editura Universităţii Suceava, 441 pp.

Huang, B., W. Angel, T. Boyer, L. Cheng, G. Chepurin, E. Freeman, C. Liu, and H.-M. Zhang, 2018: Evaluating SST analyses with independent ocean profile observations. *J. Climate*, **31**, 5015–5030, https://doi.org/10.1175/JCLI-D-17-0824.1.

InfoClima, 2024: Starea Climei – România 2024: Analiză și perspective privind schimbările climatice. 104 pp.

Ionescu, N., and M. Ionescu, 2006: Foametea din Moldova în anii 1945–1946. *Acta Moldaviae Meridionalis*, **XXV–XXVII**, 559–567.

Ionita, M., 2024: Large-scale drivers of the exceptionally low winter Antarctic sea ice extent in 2023. *Front. Earth Sci.*, **12**, 1333706, https://doi.org/10.3389/feart.2024.1333706.

——, and V. Nagavciuc, 2021: Changes in drought features at the European level over the last 120 years. *Nat. Hazards Earth Syst. Sci.*, **21**, 1685–1701, https://doi.org/10.5194/nhess-21-1685-2021.

——, and ——, 2024: Shedding light on the devastating floods in June 1897 in Romania: Early instrumental observations and synoptic analysis. *J. Hydrometeor.*, **25**, 1729–1745, https://doi.org/10.1175/JHM-D-23-0230.1.

——, G. Lohmann, and N. Rimbu, 2008: Prediction of spring Elbe discharge based on stable teleconnections with winter global temperature and precipitation. *J. Climate*, **21**, 6215–6226, https://doi.org/10.1175/2008JCLI2248.1.

——, M. Dima, G. Lohmann, P. Scholz, and N. Rimbu, 2015: Predicting the June 2013 European flooding based on precipitation, soil moisture, and sea level pressure. *J. Hydrometeor.*, **16**, 598–614, https://doi.org/10.1175/JHM-D-14-0156.1.

——, P. Scholz, K. Grosfeld, and R. Treffeisen, 2018: Moisture transport and Antarctic sea ice: Austral spring 2016 event. *Earth Syst. Dyn.*, **9**, 939–954, https://doi.org/10.5194/esd-9-939-2018.

——, M. Dima, V. Nagavciuc, P. Scholz, and G. Lohmann, 2021: Past megadroughts in central Europe were longer, more severe and less warm than modern droughts. *Commun. Earth Environ.*, **2**, 61, https://doi.org/10.1038/s43247-021-00130-w.

——, V. Nagavciuc, P. Scholz, and M. Dima, 2022: Long-term drought intensification over Europe driven by the weakening trend of the Atlantic Meridional Overturning Circulation. *J. Hydrol.*, **42**, 101176, https://doi.org/10.1016/j.ejrh.2022.101176.

——, P. Vaideanu, B. Antonescu, C. Roibu, Q. Ma, and V. Nagavciuc, 2024: Examining the Eastern European extreme summer temperatures of 2023 from a long-term perspective: The role of natural variability vs. anthropogenic factors. *Nat. Hazards Earth Syst. Sci.*, **24**, 4683–4706, https://doi.org/10.5194/nhess-24-4683-2024.

——, B. Antonescu, C. Roibu, and V. Nagavciuc, 2025a: Drought's grip on Romania: A tale of two indices. *Int. J. Climate*, **45**, e8876, https://doi.org/10.1002/joc.8876.

——, P. Vaideanu, D. Nichita, and V. Nagavciuc, 2025b: Breaking records under clear skies: The impact of sunshine duration and atmospheric dynamics on the 2024 Eastern European extreme summer temperatures. *npj Nat. Hazards*, **2**, 82, https://doi.org/10.1038/s44304-025-00137-9.

IPCC, 2021: *Climate Change 2021: The Physical Science Basis.* Cambridge University Press, 2410 pp., https://doi.org/10.1017/9781009157896.

Jackson, P., 2018: *The Mongols and the West: 1221–1410.* Routledge, 452 pp.

Jacob, D., and Coauthors, 2014: EURO-CORDEX: New high-resolution climate change projections for European impact research. *Reg. Environ. Change*, **14**, 563–578, https://doi.org/10.1007/s10113-013-0499-2.

Jones, P. D., and Coauthors, 2009: High-resolution palaeoclimatology of the last millennium: A review of current status and future prospects. *Holocene*, **19**, 3–49, https://doi.org/10.1177/0959683608098952.

Kaniewski, D., N. Marriner, F. Luce, M. Escarpe, M. Pourkerman, and T. Otto, 2025: A climate of conflict: How the little ice age sparked rebellions and revolutions across Europe. *Global Planet. Change*, **254**, 105038, https://doi.org/10.1016/j.gloplacha.2025.105038.

Kautz, L.-A., O. Martius, S. Pfahl, J. G. Pinto, A. M. Ramos, P. M. Sousa, and T. Woollings, 2022: Atmospheric blocking and weather extremes over the Euro-Atlantic sector—A review. *Wea. Climate Dyn.*, **3**, 305–336, https://doi.org/10.5194/wcd-3-305-2022.

Kingston, D. G., J. H. Stagge, L. M. Tallaksen, and D. M. Hannah, 2015: European-scale drought: Understanding connections between atmospheric circulation and meteorological drought indices. *J. Climate*, **28**, 505–516, https://doi.org/10.1175/JCLI-D-14-00001.1.

Köse, N., U. Akkemik, H. T. Güner, H. Dalfes, H. Grissino-Mayer, M. Ozeren, and T. Kındap, 2013: An improved reconstruction of May-June precipitation using tree-ring data from western Turkey and its links to volcanic eruptions. *Int. J. Biometeor.*, **57**, 691–701, https://doi.org/10.1007/s00484-012-0595-x.

Kreibich, H., and Coauthors, 2022: The challenge of unprecedented floods and droughts in risk management. *Nature*, **608**, 80–86, https://doi.org/10.1038/s41586-022-04917-5.

Laaha, G., and Coauthors, 2017: The European 2015 drought from a hydrological perspective. *Hydrol. Earth Syst. Sci.*, **21**, 3001–3024, https://doi.org/10.5194/hess-21-3001-2017.

Levanič, T., I. Popa, S. Poljanšek, and C. Nechita, 2013: A 323-year long reconstruction of drought for SW Romania based on black pine (Pinus Nigra) tree-ring widths. *Int. J. Biometeor.*, **57**, 703–714, https://doi.org/10.1007/s00484-012-0596-9.

Ljungqvist, F. C., and Coauthors, 2020: Ranking of tree-ring based hydroclimate reconstructions of the past millennium. *Quat. Sci. Rev.*, **230**, 106074, https://doi.org/10.1016/j.quascirev.2019.106074.

——, A. Seim, and H. Huhtamaa, 2021: Climate and society in European history. *Wiley Interdiscip. Rev.: Climate Change*, **12**, e691, https://doi.org/10.1002/wcc.691.

——, ——, and D. Collet, 2024: Famines in medieval and early modern Europe—Connecting climate and society. *Wiley Interdiscip. Rev.: Climate Change*, **15**, e859, https://doi.org/10.1002/wcc.859.

Loon, A. F. V., and Coauthors, 2024: Review article: Drought as a continuum—Memory effects in interlinked hydrological, ecological, and social systems. *Nat. Hazards Earth Syst. Sci.*, **24**, 3173–3205, https://doi.org/10.5194/nhess-24-3173-2024.

Luterbacher, J., and Coauthors, 2012: A review of 2000 years of paleoclimatic evidence in the Mediterranean. *The Climate of the Mediterranean Region*, P. Lionello, Ed., Elsevier, 87–185, https://doi.org/10.1016/b978-0-12-416042-2.00002-1.

Lv, P., T. Rademacher, X. Huang, B. Zhang, and X. Zhang, 2022: Prolonged drought duration, not intensity, reduces growth recovery and prevents compensatory growth of oak trees. *Agric. For. Meteor.*, **326**, 109183, https://doi.org/10.1016/j.agrformet.2022.109183.

Mészáros, I., B. Adorján, B. Nyitrai, P. Kanalas, V. Oláh, and T. Levanič, 2022: Long-term radial growth and climate-growth relationships of *Quercus petraea* (Matt.) Liebl. and *Quercus cerris* L. in a xeric low elevation site from Hungary. *Dendrochronologia*, **76**, 126014, https://doi.org/10.1016/j.dendro.2022.126014.

Mihailescu, C., 2004: *Clima și Hazardele Climatice ale Moldovei (The Climate and the Harsh Conditions of Moldova)*. Editura Știina, 192 pp.

Mikac, S., A. Žmegač, D. Trlin, V. Paulić, M. Oršanić, and I. Anić, 2018: Drought-induced shift in tree response to climate in floodplain forests of Southeastern Europe. *Sci. Rep.*, **8**, 16495, https://doi.org/10.1038/s41598-018-34875-w.

Nagavciuc, V., M. Ionita, A. Perșoiu, I. Popa, N. J. Loader, and D. McCarroll, 2019a: Stable oxygen isotopes in Romanian oak tree rings record summer droughts and associated large-scale circulation patterns over Europe. *Climate Dyn.*, **52**, 6557–6568, https://doi.org/10.1007/s00382-018-4530-7.

——, C.-C. Roibu, M. Ionita, A. Mursa, M.-G. Cotos, and I. Popa, 2019b: Different climate response of three tree ring proxies of *Pinus sylvestris* from the Eastern Carpathians, Romania. *Dendrochronologia*, **54**, 56–63, https://doi.org/10.1016/j.dendro.2019.02.007.

——, Z. Kern, M. Ionita, C. Hartl, O. Konter, J. Esper, and I. Popa, 2020: Climate signals in carbon and oxygen isotope ratios of *Pinus cembra* tree-ring cellulose from the Călimani Mountains, Romania. *Int. J. Climatol.*, **40**, 2539–2556, https://doi.org/10.1002/joc.6349.

——, M. Ionita, Z. Kern, D. McCarroll, and I. Popa, 2022a: A ~700 years perspective on the 21st century drying in the eastern part of Europe based on $\delta^{18}O$ in tree ring cellulose. *Commun. Earth Environ.*, **3**, 277, https://doi.org/10.1038/s43247-022-00605-4.

——, P. Scholz, and M. Ionita, 2022b: Hotspots for warm and dry summers in Romania. *Nat. Hazards Earth Syst. Sci.*, **22**, 1347–1369, https://doi.org/10.5194/nhess-22-1347-2022.

——, A. Mursa, M. Ionita, V. Sfeclă, I. Popa, and C.-C. Roibu, 2023a: An overview of extreme years in *Quercus* sp. Tree ring records from the northern Moldavian Plateau. *Forests*, **14**, 894, https://doi.org/10.3390/f14050894.

——, C.-C. Roibu, A. Mursa, M.-I. Știrbu, I. Popa, and M. Ionita, 2023b: The first tree-ring reconstrruction of streamflow variability over the last ~250 years in the Lower Danube. *J. Hydrol.*, **617**, 129150, https://doi.org/10.1016/j.jhydrol.2023.129150.

——, and Coauthors, 2024: A past and present perspective on the European summer vapor pressure deficit. *Climate Past*, **20**, 573–595, https://doi.org/10.5194/cp-20-573-2024.

——, G. Helle, M. Rădoane, C.-C. Roibu, M.-G. Cotos, and M. Ionita, 2025: A long-term drought reconstruction based on oxygen isotope tree ring data for central and eastern parts of Europe (Romania). *Biogeosciences*, **22**, 55–69, https://doi.org/10.5194/bg-22-55-2025.

Nechita, C., K. Čufar, I. Macovei, I. Popa, and O. N. Badea, 2019: Testing three climate datasets for dendroclimatological studies of oaks in the South Carpathians. *Sci. Total Environ.*, **694**, 133730, https://doi.org/10.1016/j.scitotenv.2019.133730.

Osborn, T. J., K. R. Biffa, and P. D. Jones, 1997: Adjusting variance for sample-size in tree-ring chronologies and other regional-mean timeseries. *Dendrochronologia*, **15**, 89–99.

Pauling, A., J. Luterbacher, C. Casty, and H. Wanner, 2006: Five hundred years of gridded high-resolution precipitation

reconstructions over Europe and the connection to large-scale circulation. *Climate Dyn.*, **26**, 387–405, https://doi.org/10.1007/s00382-005-0090-8.

Petritan, A. M., I. C. Petritan, A. Hevia, H. Walentowski, O. Bouriaud, and R. Sánchez-Salguero, 2021: Climate warming predispose sessile oak forests to drought-induced tree mortality regardless of management legacies. *For. Ecol. Manage.*, **491**, 119097, https://doi.org/10.1016/j.foreco.2021.119097.

Pfister, C., and H. Wanner, 2021: *Climate and Society in Europe the Last Thousand Years.* Haupt Verlag, 396 pp.

Pinke, Z., L. Ferenczi, B. F. Romhányi, J. Laszlovszky, and S. Pow, 2017: Climate of doubt: A re-evaluation of Büntgen and Di Cosmo's environmental hypothesis for the Mongol withdrawal from Hungary, 1242 CE. *Sci. Rep.*, **7**, 12695, https://doi.org/10.1038/s41598-017-12128-6.

Popa, I., and Z. Kern, 2009: Long-term summer temperature reconstruction inferred from tree-ring records from the Eastern Carpathians. *Climate Dyn.*, **32**, 1107–1117, https://doi.org/10.1007/s00382-008-0439-x.

Roibu, C.-C., V. Sfeclă, A. Mursa, M. Ionita, V. Nagavciuc, F. Chiriloaei, I. Leşan, and I. Popa, 2020: The climatic response of tree ring width components of ash (*Fraxinus excelsior* L.) and common oak (*Quercus robur* L.) from Eastern Europe. *Forests*, **11**, 600, https://doi.org/10.3390/f11050600.

——, T. Ważny, A. Crivellaro, A. Mursa, F. Chiriloaei, M.-I. I. Ştirbu, and I. Popa, 2021: The Suceava oak chronology: A new 804 years long tree-ring chronology bridging the gap between central and south Europe. *Dendrochronologia*, **68**, 125856, https://doi.org/10.1016/j.dendro.2021.125856.

——, V. Nagavciuc, M. Ionita, I. Popa, S.-A. Horodnic, A. Mursa, and U. Büntgen, 2022: A tree ring-based hydroclimate reconstruction for eastern Europe reveals large-scale teleconnection patterns. *Climate Dyn.*, **59**, 2979–2994, https://doi.org/10.1007/s00382-022-06255-8.

Ruffinatto, F., and A. Crivellaro, 2019: *Atlas of Macroscopic Wood Identification.* Springer International Publishing, 439 pp.

Skiadaresis, G., J. Schwarz, K. Stahl, and J. Bauhus, 2021: Groundwater extraction reduces tree vitality, growth and xylem hydraulic capacity in *Quercus robur* during and after drought events. *Sci. Rep.*, **11**, 5149, https://doi.org/10.1038/s41598-021-84322-6.

Slivinski, L. C., and Coauthors, 2019: Towards a more reliable historical reanalysis: Improvements for version 3 of the Twentieth Century Reanalysis system. *Quart. J. Roy. Meteor. Soc.*, **145**, 2876–2908, https://doi.org/10.1002/qj.3598.

Sochová, I., T. Kolář, and M. Rybníček, 2021: A review of oak dendrochronology in eastern Europe. *Tree. Ring Res.*, **77**, 10–19, https://doi.org/10.3959/TRR2020-2.

——, and Coauthors, 2024: The palaeoclimatic potential of recent oak tree-ring width chronologies from Southwest Ukraine. *Dendrochronologia*, **84**, 126168, https://doi.org/10.1016/j.dendro.2024.126168.

Solomina, O., N. Davi, R. D'Arrigo, and G. Jacoby, 2005: Tree-ring reconstruction of Crimean drought and lake chronology correction. *Geophys. Res. Lett.*, **32**, L19704, https://doi.org/10.1029/2005GL023335.

Stănescu, V., 1979: *Dendrologie.* Editura Didactică şi Pedagogică, 470 pp.

Storch, H. V., and F. W. Zwiers, 1999: *Statistical Analysis in Climate Research.* Cambridge University Press, 484 pp., https://doi.org/10.1017/cbo9780511612336.

Stothers, R. B., 1999: Volcanic dry fogs, climate cooling, and plague pandemics in Europe and the Middle East. *Climatic Change*, **42**, 713–723, https://doi.org/10.1023/A:1005480105370.

Tegel, W., J. Vanmoerkerke, and U. Büntgen, 2010: Updating historical tree-ring records for climate reconstruction. *Quat. Sci. Rev.*, **29**, 1957–1959, https://doi.org/10.1016/j.quascirev.2010.05.018.

Teodoreanu, E., 2017: *În căutarea timpului trecut Schiă de climatologie istorică.* Editura Paodeia, 363 pp.

Toohey, M., and M. Sigl, 2017: Volcanic stratospheric sulfur injections and aerosol optical depth from 500 BCE to 1900 CE. *Earth Syst. Sci. Data*, **9**, 809–831, https://doi.org/10.5194/essd-9-809-2017.

Topor, N., 1963: *Anii ploioşi şi secetoşi din Republica Populară Romînă.* C.S.A Institutul Meteorologic, 304 pp.

Touchan, R., E. Xoplaki, G. Funkhouser, J. Luterbacher, M. K. Hughes, N. Erkan, Ü. Akkemik, and J. Stephan, 2005: Reconstructions of spring/summer precipitation for the eastern Mediterranean from tree-ring widths and its connection to large-scale atmospheric circulation. *Climate Dyn.*, **25**, 75–98, https://doi.org/10.1007/s00382-005-0016-5.

Tumajer, J., and V. Treml, 2016: Response of floodplain pedunculate oak (*Quercus robur* L.) tree-ring width and vessel anatomy to climatic trends and extreme hydroclimatic events. *For. Ecol. Manage.*, **379**, 185–194, https://doi.org/10.1016/j.foreco.2016.08.013.

Twardosz, R., and U. Kossowska-Cezak, 2013: Exceptionally hot summers in Central and Eastern Europe (1951–2010). *Theor. Appl. Climatol.*, **112**, 617–628, https://doi.org/10.1007/s00704-012-0757-0.

Vicente-Serrano, S. M., and Coauthors, 2025: High temporal variability not trend dominates Mediterranean precipitation. *Nature*, **639**, 658–666, https://doi.org/10.1038/s41586-024-08576-6.

Wazny, T., and D. Eckstein, 1991: The dendrochronological signal of oak (*Quercus spp.*) in Poland. *Dendrochronologia*, **9**, 181–191.

Wigley, T. M. L., K. R. Briffa, and P. D. Jones, 1984: On the average value of correlated time series, with applications in dendroclimatology and hydrometeorology. *J. Climate Appl. Meteor.*, **23**, 201–213, https://doi.org/10.1175/1520-0450(1984)023<0201:OTAVOC>2.0.CO;2.

Wilson, R. J. S., B. H. Luckman, and J. Esper, 2005: A 500 year dendroclimatic reconstruction of spring–summer precipitation from the lower Bavarian Forest region, Germany. *Int. J. Climatol.*, **25**, 611–630, https://doi.org/10.1002/joc.1150.

Xoplaki, E., and Coauthors, 2016: The Medieval Climate Anomaly and Byzantium: A review of the evidence on climatic fluctuations, economic performance and societal change. *Quat. Sci. Rev.*, **136**, 229–252, https://doi.org/10.1016/j.quascirev.2015.10.004.

Xu, G., and Coauthors, 2024: Jet stream controls on European climate and agriculture since 1300 CE. *Nature*, **634**, 600–608, https://doi.org/10.1038/s41586-024-07985-x.

Yue, W., and Coauthors, 2026: Drought facilitated the westward expansion of the Mongol Empire in the 1230s. *Fundam. Res.*, https://doi.org/10.1016/j.fmre.2025.08.010, in press.

Zang, C., and F. Biondi, 2015: treeclim: An R package for the numerical calibration of proxy-climate relationships. *Ecography*, **38**, 431–436, https://doi.org/10.1111/ecog.01335.

Zhang, D. D., H. F. Lee, C. Wang, B. Li, Q. Pei, J. Zhang, and Y. An, 2011: The causality analysis of climate change and large-scale human crisis. *Proc. Natl. Acad. Sci. USA*, **108**, 17 296–17 301, https://doi.org/10.1073/pnas.1104268108.